

History and features of trans-oceanic tsunamis and implications for paleo-tsunami studies



Kenji Satake^{a,*}, Mohammad Heidarzadeh^b, Marco Quiroz^{c,d}, Rodrigo Cienfuegos^{c,d}

^a Earthquake Research Institute, the University of Tokyo, Yayoi, Bunkyo-ku, Tokyo 113-0032, Japan

^b Department of Civil & Environmental Engineering, Brunel University London, Uxbridge UB8 3PH, UK

^c Departamento de Ingeniería Hidráulica y Ambiental, Pontificia Universidad Católica de Chile, Santiago, Chile

^d Centro de Investigación para la Gestión Integrada del Riesgo de Desastres (CIGIDEN Conicyt/Fondap/15110017), Chile

ARTICLE INFO

Keywords:

Tsunami
Earthquake
Subduction zone
Tide gauge
Historical document
Paleo-tsunami
Numerical modeling

ABSTRACT

Far-field tsunamis and their features, as well as methods to quantify trans-oceanic tsunamis are reviewed, with examples of instrumental and historical data. Tsunamis from the 1854 Nankai earthquakes, the 1946 Aleutian tsunami earthquake, the 1960 and 2010 Chile earthquakes, as well as the 2011 Tohoku earthquake, were recorded around the Pacific Ocean. The 1883 Krakatoa volcanic eruption caused volcanic tsunamis in the Indian Ocean and meteotsunami in the Pacific Ocean. The 2004 Indian Ocean tsunami was also recorded in the Pacific Ocean. When a tsunami amplitude is larger than that of ocean tides, which usually requires the parent earthquake to be gigantic ($M_w \sim 9$), it can cause damage and may be historically documented. The trans-Pacific tsunamis described in historical documents include those from the 1700 Cascadia earthquake, the 1730, 1751, 1837, and 1877 earthquakes off Chile, and the 1687 and 1868 earthquakes off Peru. The tsunami record in Japan from the 1586 Peru earthquakes was found to be incorrect and should be discounted. The tsunami magnitude scale relates the tsunami heights to the earthquake size. Tsunami travel time can be computed from actual bathymetry, and the tsunami ray tracing provides relative amplitudes, due to focusing/defocusing caused by irregular bathymetry. Numerical computations from fault models produce tsunami amplitudes and waveforms, and indicate strong directivity due to strike of fault or orientation of subduction zones. Far-field tsunamis are often long-lasting, due to multiple reflections across the basin or on continental shelf, or due to resonance in bays/harbors. These features would provide important criteria to estimate tsunami sources from paleo-tsunami data.

1. Introduction

Unlike other geo-hazards, tsunamis can cause damage across the oceans, as demonstrated by the 2004 Indian Ocean tsunami, which caused damage and death in 14 countries around the Indian Ocean (Satake, 2014). Trans-oceanic tsunamis from giant earthquakes or volcanic eruptions have been recorded either instrumentally or in historical documents.

In studies of past tsunami deposits, the tsunami sources are sometimes considered in far-field across the oceans. For example, prehistoric tsunami deposits in the Hawaiian Islands are attributed to the Aleutian source(s) (La Selle et al., 2019). Butler et al. (2017) estimated the age of coral boulders in Hawaii as 1572 CE \pm 21, and correlated it to the 1586 tsunami record in Japan. While the 1586 Japanese tsunami was believed to be from the Peru earthquake, Butler et al. (2017) proposed an Aleutian origin for it. We will show in Section 3.3 that the 1586

tsunami record in Japan was incorrect.

In order to reliably estimate the source of prehistoric tsunami deposit, we need to understand the characteristics of trans-oceanic tsunamis. In this paper, we first review, in Section 2, recent (a few centuries) trans-oceanic tsunamis that were instrumentally recorded. In Section 3, we review trans-oceanic tsunamis that were historically documented. In Section 4, we summarize tsunami modeling methods with recent developments, and finally, in Section 5, we discuss characteristic features of trans-oceanic tsunamis and their implication to paleo-tsunami studies.

2. Instrumentally recorded trans-oceanic tsunamis

In this section, we discuss a number of instrumentally-recorded tsunamis with trans-oceanic propagation. The two tsunamis from the 1854 Nankai earthquakes were recorded in California; the 1883

* Corresponding author.

E-mail addresses: satake@eri.u-tokyo.ac.jp (K. Satake), Mohammad.Heidarzadeh@brunel.ac.uk (M. Heidarzadeh), mquiroz@uc.cl (M. Quiroz), racienfu@ing.puc.cl (R. Cienfuegos).

<https://doi.org/10.1016/j.earscirev.2020.103112>

Received 26 September 2019; Received in revised form 25 January 2020; Accepted 30 January 2020

Available online 31 January 2020

0012-8252/ © 2020 Elsevier B.V. All rights reserved.

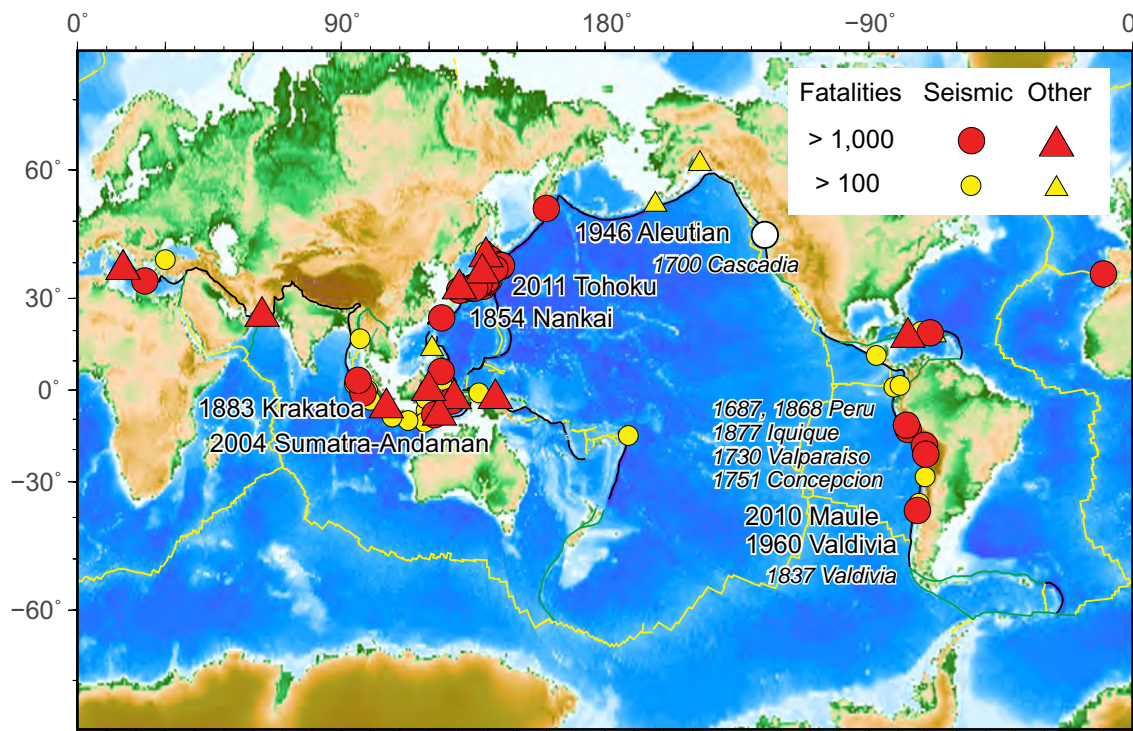


Fig. 1. Worldwide distribution of sources of damaging tsunamis. Symbols represent the historical events with validity = 4 (definite tsunami) with > 100 (yellow) or 1000 > (red) casualties. Circles are tsunami sources with earthquake origin and triangles are those with non-seismic origin. Symbols with text labels are mentioned and discussed in this article. The data are from NGDC/WDS Global Historical Tsunami Database, <https://doi.org/10.7289/V5PN93H7>. (For interpretation of the references to colour in this figure legend, the reader is referred to the web version of this article.)

Krakatoa volcanic eruption was recorded as a volcanic tsunami in the Indian Ocean and as a meteotsunami in the Pacific Ocean; unusual tsunami from the 1946 Aleutian earthquake was recorded in Hawaii and other Pacific islands; large tsunamis from the 1960 and 2010 Chile earthquakes, as well as the tsunami from the 2011 Tohoku earthquake, were recorded around the Pacific Ocean; and the 2004 Indian Ocean tsunami was recorded at a global scale (Fig. 1). Besides the aforesaid events, tsunamis from gigantic earthquakes in the 20th century, such as the 1906 Colombia-Ecuador earthquake (Yoshimoto et al., 2017), the 1957 Aleutian earthquake (Johnson et al., 1994), and the 1964 Alaska earthquake (Johnson et al., 1996), were also recorded in the Pacific Ocean. Abe (1979) compiled the far-field tsunami amplitudes and assigned tsunami magnitude, as we describe in later Section 4.1.

For tsunami waveforms, which is instrumentally recorded on sea level gauges, we use “tsunami amplitude”, measured from zero to either crest (positive peak) or trough (negative peak) of the wave. We avoid using the term “wave height”, which is referred to the trough-to-crest height of the wave. The height of tsunami measured or documented on land can be either inundation height (measured relative to the sea level) or run-up height (at the maximum inundation distance); hence, we simply call it “tsunami height”.

2.1. The 1854 Nankai earthquakes

The oldest instrumentally recorded trans-Pacific tsunamis are those recorded in California, from the 1854 Tokai and Nankai earthquakes. These events were the penultimate series of the great interplate earthquakes along the Nankai trough, that have shown a recurrence interval of 90–150 years (Satake, 2015b). The 1854 Tokai earthquake (M 8.4) occurred at ~ 9 am (local time, or ~ 0:00 UTC) on December 23, followed by the Nankai earthquake (M 8.4), which occurred ~ 30 h later. These earthquakes caused up to 10 m high tsunami in Japan, as inferred from historical documents (Earthquake Research Committee, 2013). The tsunami waves were recorded on a tide gauge at San Francisco,

operated by the U.S. Coast Survey (Bache, 1856) (Fig. 2). From ~ 4 am (12:30 UTC), or ~ 12.5 h after the earthquake, the record shows long-lasting (~ 18 h) oscillations with average period of ~ 30 min, and maximum amplitudes of ~ 10 cm, much smaller than the tidal amplitudes of ~ 2 m. Another long-lasting sea disturbance from the Nankai earthquake followed ~ 30 h later (Fig. 2). While the tide gauge record at San Diego also shows similar long-lasting oscillations, the record at Astoria, Oregon, shows little disturbance of no more than a few centimeters; hence the long-lasting oscillations at San Francisco and San Diego may represent oscillations of respective bays, due to the incoming trans-Pacific tsunamis.

2.2. The 1883 Krakatoa volcano eruption tsunami

The 1883 eruption of the Krakatoa volcano, in Indonesia, is one of the largest volcanic eruptions recorded in human history. The eruption refaced the island of Krakatoa; the northern portion of the island was replaced by a caldera, up to 270 m deep (Simkin and Fiske, 1983). The eruption also generated tsunamis, with maximum heights of 15 m, that destroyed nearby coastal villages and took ~ 36,000 lives along the Sunda Strait. The tsunami was recorded on a tide gauge at Batavia (now Jakarta) with a maximum amplitude of at least 1 m, and on gauges in the Indian Ocean countries, i.e., India, Australia, and South Africa, with amplitudes of several tens of centimeters (Pelinovsky et al., 2005). The arrival times of these tsunamis were roughly reproduced by ray tracing and hydrodynamic modeling (see Section 4) (Choi et al., 2003). The sea disturbances were also recorded on tide gauges in the Pacific Ocean, i.e., San Francisco and Honolulu, with maximum amplitudes of up to 10 cm (Fig. 3), but they were considered as meteotsunamis; the arrival times of these sea level disturbances were too early, by more than several hours, to be explained as tsunami (long waves), and they were modeled by sea waves coupled by air waves from the eruption (Ewing and Press, 1955; Press and Harkrider, 1966).

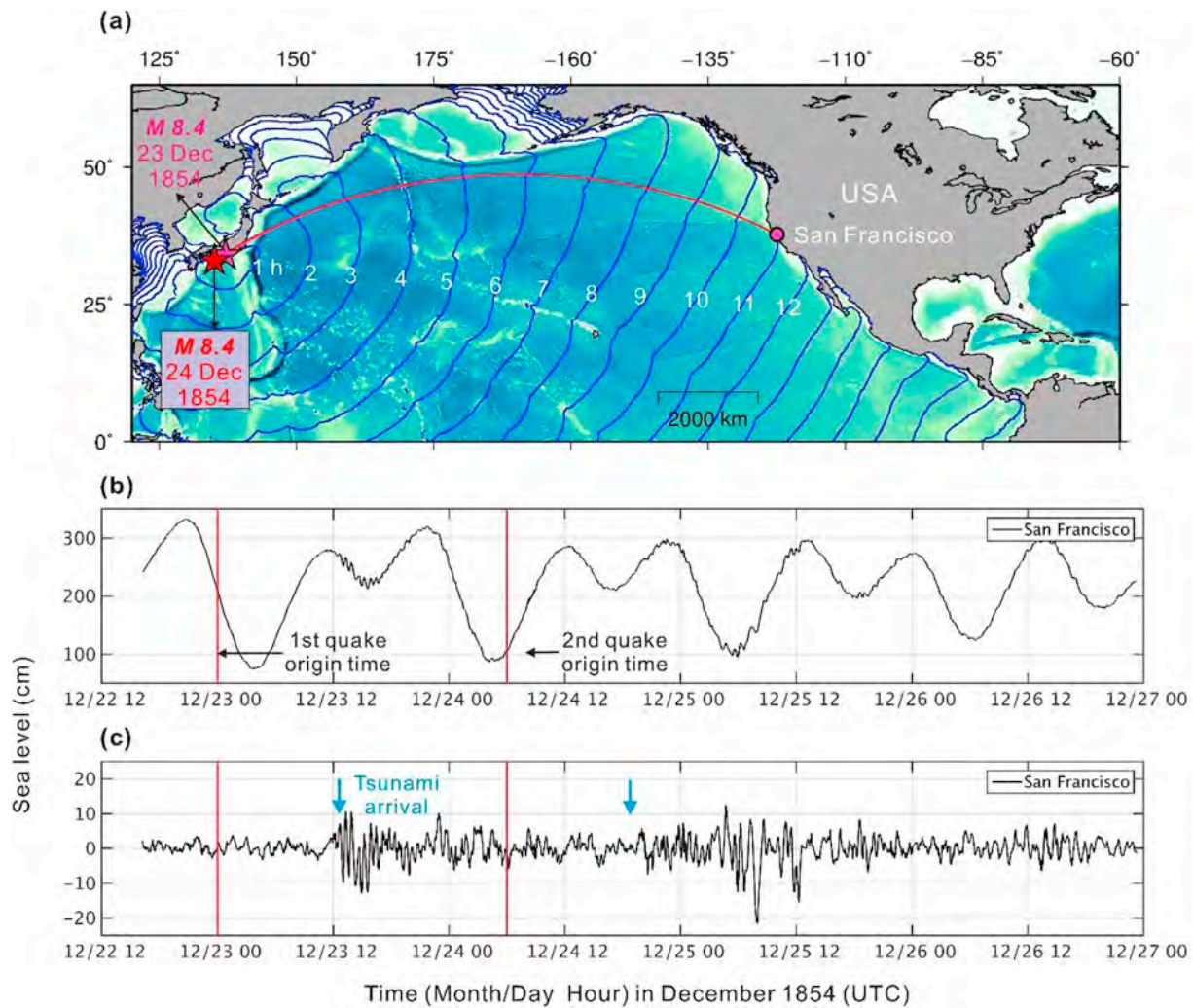


Fig. 2. (a) Tsunami travel times from the 1854 Tokai and Nankai earthquakes. (b) Tide gauge record at San Francisco, California, in December 1854, including tsunami signal from the Tokai and Nankai earthquakes. Waveforms are digitized and stored by NOAA, National Center for Environmental Information <https://www.ngdc.noaa.gov/hazard/tide.shtml>. (c) Tidal components are removed from (b). Tsunami arrivals (blue arrows), ~ 12.5 h after the earthquake origin times, and following oscillations are shown. (For interpretation of the references to colour in this figure legend, the reader is referred to the web version of this article.)

2.3. The 1946 Aleutian earthquake tsunami

The 1946 Aleutian earthquake was unusual; the earthquake generated huge tsunami (up to ~ 40 m high) near the Aleutians, even though its surface wave magnitude (M_S) was only 7.4. This is a typical example of a “tsunami earthquake”, which generates much larger tsunamis than expected from its seismic waves (Kanamori, 1972).

The tsunami arrived in Hawaii in the morning of April 1, 1946, ~ 4.5 h after the earthquake, causing more than 150 deaths in the Hawaiian Islands (Macdonald et al., 1947). On the northern coast of Hawaii Island (Big Island), where the reported tsunami height was 17 m, one of the two sand layers extending inland, up to 350 m from the coast, was attributed to tsunami deposit from this earthquake (Chagué-Goff et al., 2012). The tsunami was also documented as high as 10 m and caused damage in other islands in the Pacific Ocean, such as Marquesas, Easter Island (Okal et al., 2002).

The tsunami was also recorded on tide gauges in Hawaii and the west coasts of USA and Canada, and such sea level records were used to analyze the tsunami source and its coastal behaviors (Green, 1946; Johnson and Satake, 1997; Rabinovich et al., 2019). The tsunami amplitudes on tide gauges were less than 0.6 m, smaller than the tidal range, at most stations.

2.4. The 1960 and 2010 Chile tsunamis

The 1960 Chile (Valdivia) earthquake was the largest instrumentally-recorded earthquake ($M_w = 9.5$). The tsunami propagated across the Pacific Ocean, reached the Hawaiian Islands in 15 h, and caused 61 casualties there. The average tsunami height was 3 m in Hawaii, but it was more than 10 m in Hilo (Eaton et al., 1961). The tsunami further propagated across the Pacific Ocean, reached Japan in ~ 23 h, leaving 139 casualties (JMA, 1961). The tsunami was recorded at many tide gauges around the Pacific Ocean (Berkman and Symons, 1964; Rabinovich et al., 2019), which have been used to study the earthquake source (Ho et al., 2019). The distribution of tsunami amplitudes on tide gauges (Fig. 4) shows that the far-field tsunami was the largest in Japan, and was also large on the west coast of USA, Canada, New Zealand, the Philippines, and Hawaii.

In Japan, the tsunami heights were mostly in the range of 2–4 m, but were locally 5–6 m due to wave amplitude amplification in embayments. In Miyako bay (Fig. 5), a narrow U-shaped bay with a length of ~10 km and an average depth of 20 m, local tsunami heights varied significantly, due to resonance effect of the bay (see Section 4.4). Near the entrance of the bay, where the tide gauge station is located, the tsunami heights were less than 2 m. Around the most inner part of the bay, the tsunami height was ~ 6 m, and the tsunami's scouring and

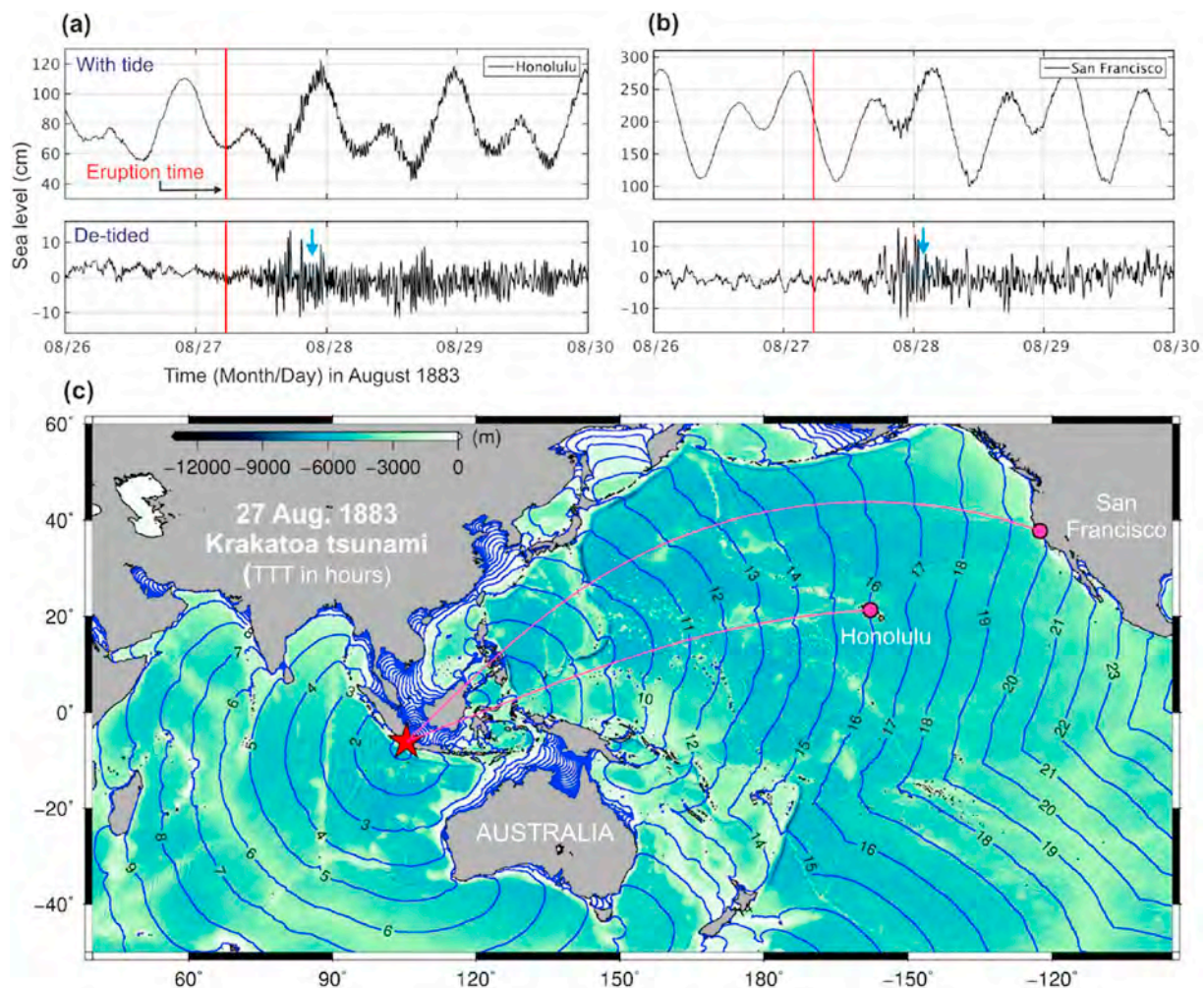


Fig. 3. (a), (b) Tide gauge records (original and de-tided) at Honolulu and San Francisco, following the 1883 Krakatoa eruption. Note that tsunamis are expected at 16 h and 20 h after the origin time (the blue arrows), while the sea level disturbances started much earlier. (c) Map shows computed tsunami travel time contours with 1 h intervals.

deposition, probably the first description of tsunami deposit, was reported (Konno et al., 1961).

The 2010 Chile (also known as Maule) earthquake (Mw 8.8) occurred just north of the 1960 source. The tsunami was recorded at many tide gauges around the Pacific Ocean, as well as at 25 bottom pressure gauges of the Deep Ocean Assessment and Reporting of Tsunamis (DART) systems operated by the National Oceanic and Atmospheric Administration (NOAA) of the USA. The tsunami amplitudes ranged from a few to several tens of cm. The tsunami height in Japan was up to 2 m, much smaller than that of the 1960 tsunami.

In addition to the 1960 and 2010 earthquakes, other recent earthquakes in Chile, namely the 1985 Valparaiso (Mw 8.0), 1995 Antofagasta (Mw 8.1), 2014 Iquique (Mw 8.2) (Gusman et al., 2015), and 2015 Illapel (Mw 8.3) (Heidarzadeh et al., 2016) earthquakes, also generated tsunamis that were recorded on tide gauges in Japan. From the comparison of these tsunami amplitudes and the size of the earthquakes, Carvajal et al. (2017a) derived an empirical relationship of $M_w = 1.26 \log_{10} H + 8.8$, where H is the tsunami amplitude in meters. This relation can be used to estimate size of historical earthquakes from tsunami heights (see Section 3).

2.5. The 2004 Indian Ocean tsunami

The 2004 Sumatra-Andaman earthquake (Mw 9.1) occurred off the coast of Sumatra Island on December 26, 2004, generating a tsunami

that devastated the shores of the Indian Ocean. The total casualties were 228,000, from 14 countries, making it the worst tsunami disaster in historical time (Satake, 2014). After attacking the nearby Sumatra Island, the tsunami reached the coasts of Thailand, Sri Lanka, and India in ~ 2 h after the earthquake. The tsunami further propagated across the Indian Ocean, then into the Atlantic and Pacific Oceans, and was recorded on tide gauges globally (Titov et al., 2005; Fig. 6).

The tsunami heights measured by field surveys were 5 to 15 m in Thailand and Sri Lanka, and up to 5 m near India's Andaman Islands (Satake, 2014, 2015a). The tsunami amplitudes on tide gauges were from 0.5 to 3 m in Indian Ocean (Rabinovich and Thomson, 2007), and > 0.5 m at some stations in the Atlantic and Pacific Oceans (Rabinovich et al., 2006).

The tsunami propagation in deep water was also captured by other devices such as bottom pressure gauges (Rabinovich et al., 2017; Heidarzadeh and Satake, 2013), satellite altimeters (Smith et al., 2005), hydrophones (Hanson et al., 2007), and horizontal components of broad-band seismographs (Yuan et al., 2005).

The 2004 Indian Ocean tsunami left various deposits, from sand to boulder, in Thailand (e.g., Goto et al., 2007; Jankaew et al., 2008), Sri Lanka (e.g., Morton et al., 2008), and India (e.g., Narayana et al., 2007). These modern tsunami deposits were studied for their characteristics, and the knowledge was used to identify paleo-tsunami deposits to infer prehistoric earthquakes.

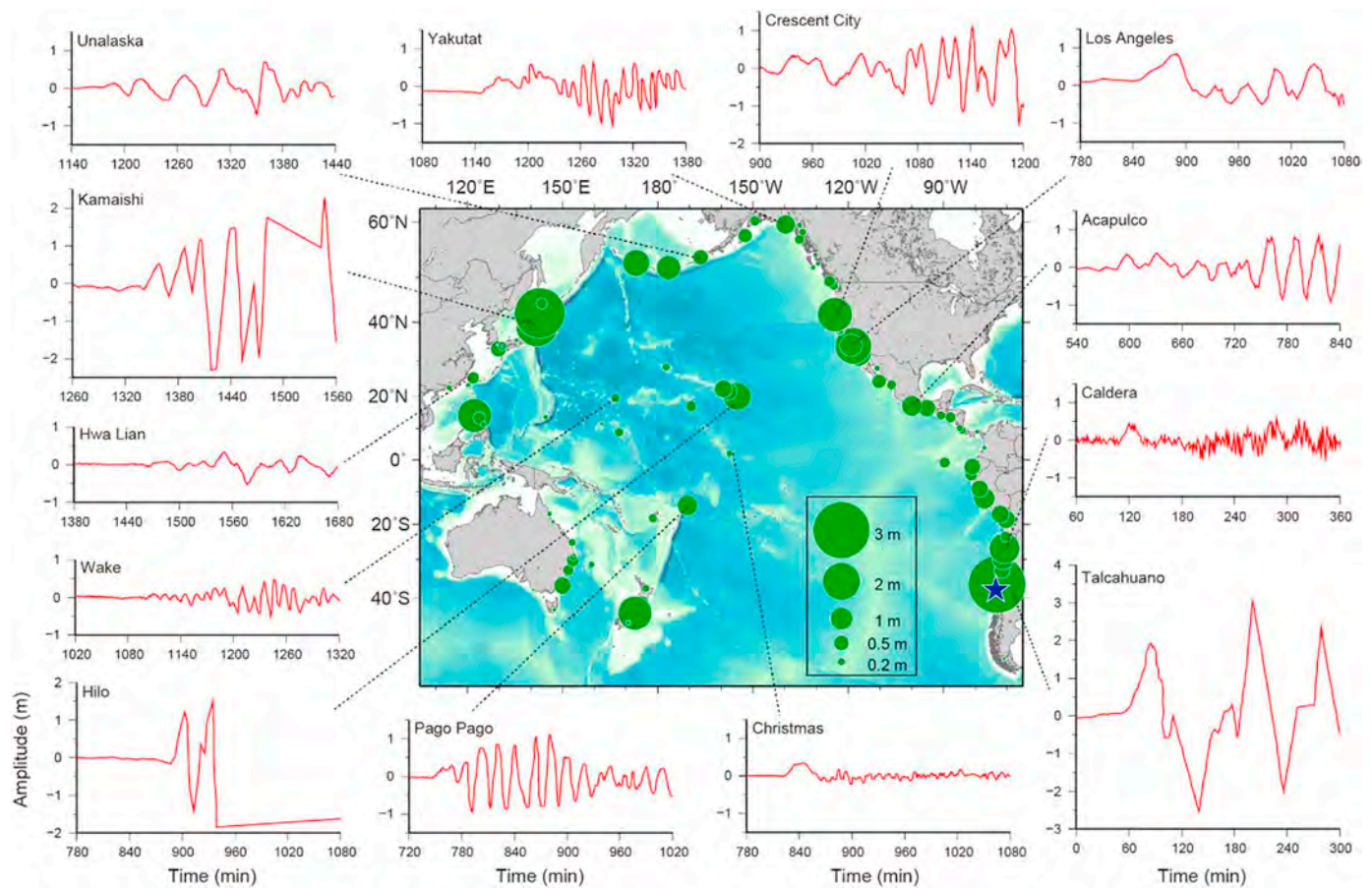


Fig. 4. The central map shows maximum amplitudes of observed tsunami waveforms (green circles) from the 1960 Chile earthquake (epicenter is shown by blue star). The tsunami waveforms recorded on tide gauges around the Pacific Ocean are also shown, with the time measured from the earthquake origin time. Based on Fujii and Satake (2013). (For interpretation of the references to colour in this figure legend, the reader is referred to the web version of this article.)

2.6. The 2011 Tohoku tsunami

The March 2011 Tohoku earthquake (Mw 9.0), which occurred off the northern coast of Honshu, was the largest instrumentally-recorded earthquake in Japan and caused a devastating tsunami disaster. The maximum tsunami run-up heights were ~ 40 m (Tsuji et al., 2014), and > 10 m tsunami heights extended along ~ 400 km of the Pacific coast of Japan. The tsunami then propagated across the Pacific Ocean and caused two casualties outside Japan, one in Indonesia and the other in USA.

The tsunami was also recorded by the bottom pressure gauges of DART and coastal gauges throughout the Pacific Ocean (Fig. 7). The maximum tsunami amplitudes were ~ 1.5 m on the west coast of USA and ~ 2 m along the southern coast of Chile (Heidarzadeh and Satake, 2013). The tsunami propagation across the Pacific Ocean was also detected as Sea Surface Height by three satellites (Ho et al., 2017).

Fig. 8 compares tsunami waveforms recorded at Coquimbo, Chile, tide gauge station from the 2015 Illapel earthquake, the 2010 Maule earthquake, and the 2011 Tohoku earthquake. The recorded tsunami amplitude was the largest, ~ 4 m, from the nearby Illapel earthquake, but it decayed quickly and became ~ 1 m, similar to a tidal variation, in ~ 8 h. The tsunami waveform from the 2010 Maule earthquake shows large amplitude (> 1 m) lasting ~ 6 h at regional distances. The tsunami waveforms from the trans-Pacific Tohoku earthquake showed that the largest amplitude of ~ 2 m appeared ~ 3 h after the first arrival (amplitude comparable to the one resulted from the 2010 earthquake), and lasted ~ 9 h. The long-lasting tsunami was due to multiple reflections of incoming wave on the continental shelf (see Section 4.4).

3. Historically recorded trans-oceanic tsunamis

Trans-Pacific tsunamis originated off North and South America were recorded in historical documents in Japan. The Japanese tsunami data were used to estimate the origin time and size of the 1700 Cascadia earthquake. Tsunamis from historical earthquakes in Chile were also recorded in Japan due to favorable directivity. The earthquakes in Peru have weaker tsunami directivity towards Japan, compared to the Chilean earthquakes, but cause strong signals towards New Zealand. The 1586 tsunami from Peru was not recorded in Japan.

In historical documents, water levels on coast or land are described or can be inferred from tsunami damage. In order to estimate the real tsunami heights, we need to consider the tide level at the time of tsunami arrivals at the coast. If the tsunami arrived at low tide, the tsunami height must be larger than that arrived at high tide, in order to cause the damage. The tide level can be computed if the date and time are known, using the tide harmonics of the present day (Fig. 9).

3.1. The 1700 Cascadia earthquake tsunami

The Cascadia subduction zone along the Pacific Northwest of the USA and Canada is a typical subduction zone, where the Juan de Fuca plate subducts beneath the North American plate, but occurrence of great interplate earthquakes has not been documented since the region's written history began in the 1800's. Paleo-seismological studies, which started in the 1980's, have found geological evidence of past earthquakes, such as buried peat layers and ghost forest indicating coastal subsidence, as well as traces of liquefaction and tsunami deposits (Atwater et al., 2015). Geological and tree-ring evidence indicate that

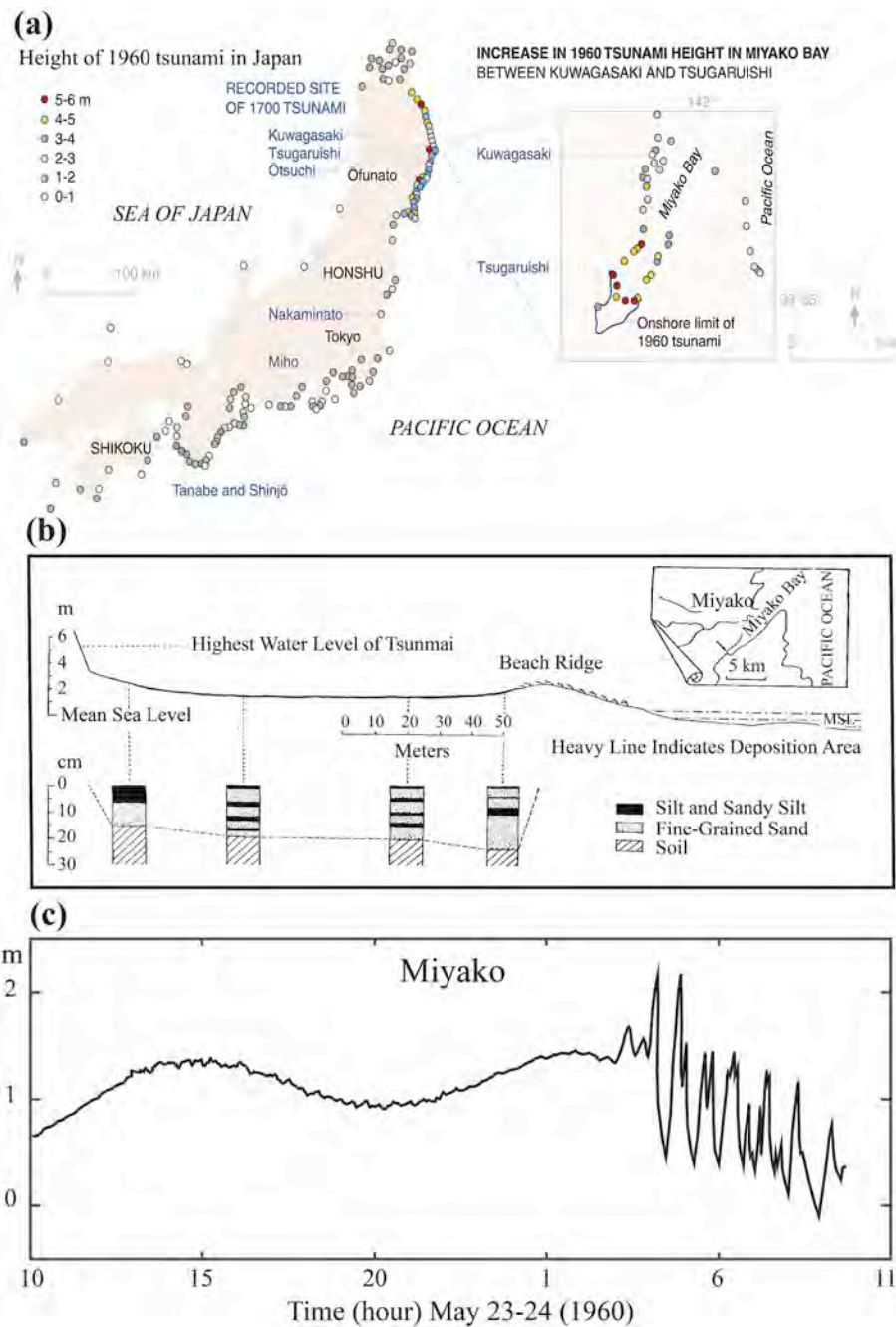


Fig. 5. The 1960 Chile earthquake tsunami recorded in Japan. (a) The tsunami heights along the Japanese coast and around Miyako bay (Atwater et al., 2015). (b) The tsunami deposit reported near Kanahama (Konno et al., 1961). (c) The tsunami waveform recorded at Miyako tide gauge station, located near the entrance of the bay (JMA, 1961). Time is in local time (JST = UTC + 9 h).

the most recent earthquake along the Cascadia subduction zone took place ~ 300 years ago, which was prehistorical time with no written records in North America, but was historical time in some other countries such as Japan.

Tsunamis without parent earthquakes, presumably the trans-Pacific tsunamis, were reported in six independent historical documents in Japan in January 1700. The earliest tsunami arrived at midnight of January 28 in Miyako (Kuwagasaki), when the tide level was slightly lower than the mean sea level (Fig. 9), causing damage to houses and rice paddies in Kuwagasaki, Tsugaruishi, and Otsuchi, on the Sanriku coast of Japan. In Nakaminato, a rice boat was not able to enter the port due to high waves and two crew members were lost. In Miho (central Japan) and Tanabe (western Japan), unusual tsunami inundation was

documented. Based on these damage and inundation descriptions, and the comparison with the 1960 Chile tsunami, the 1700 tsunami heights were estimated as 2–5 m (Fig. 10). Comparison of these estimated tsunami heights with numerical simulations (see Section 4) from fault model in Cascadia subduction zone, enabled an estimation of the time and the size of the earthquake, being ~ 9 pm January 26 (local time) and $M_w = 8.7$ – 9.2 , respectively (Satake et al., 1996, 2003).

3.2. Tsunamis from historical earthquakes in Chile

Along nearly 3000-km coast of Chile, extending from the Peruvian border (latitude 18°S) to the southern edge of Nazca plate (latitude 46°S), many subduction-zone earthquakes have occurred (Fig. 11).

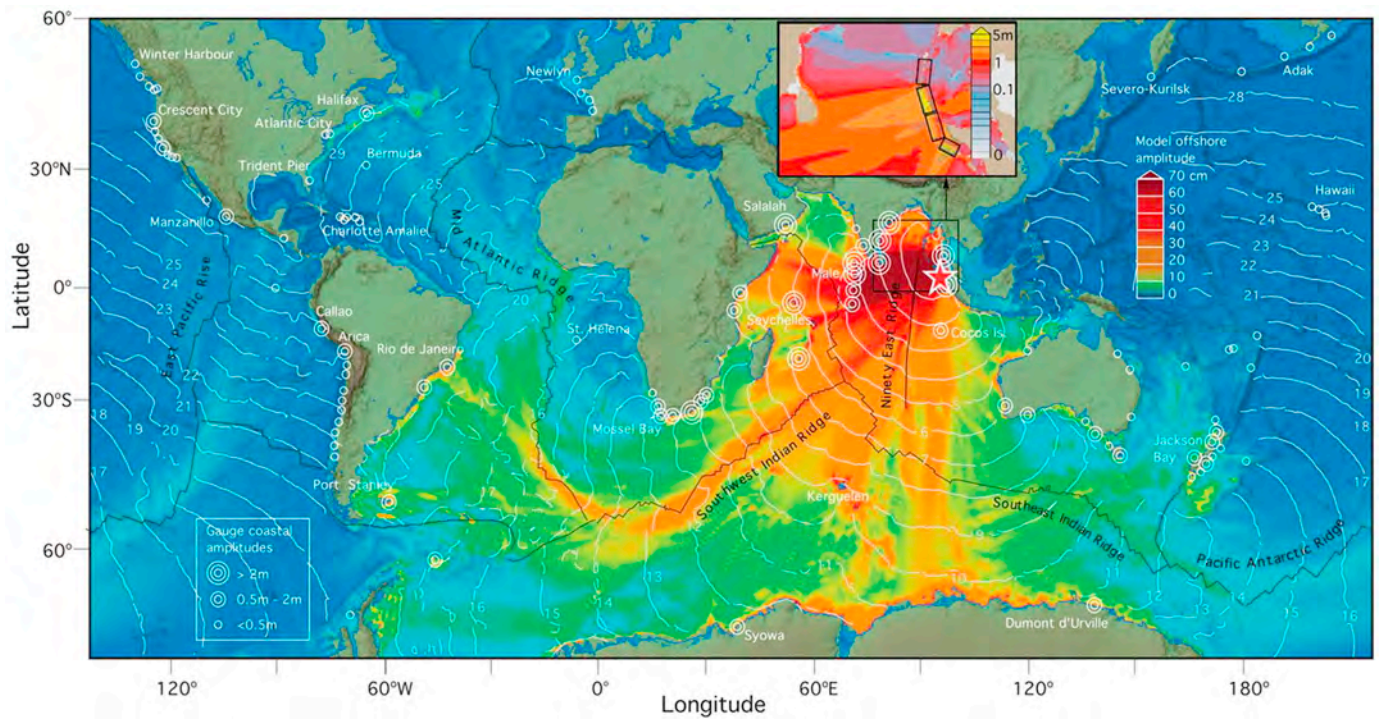


Fig. 6. Tsunami amplitudes (colour) computed from a fault model (inset) of the 2004 Sumatra-Andaman earthquake, with the computed travel times (white curves), and the locations and amplitudes of the observed tsunami data. Reproduced from Titov et al. (2005).

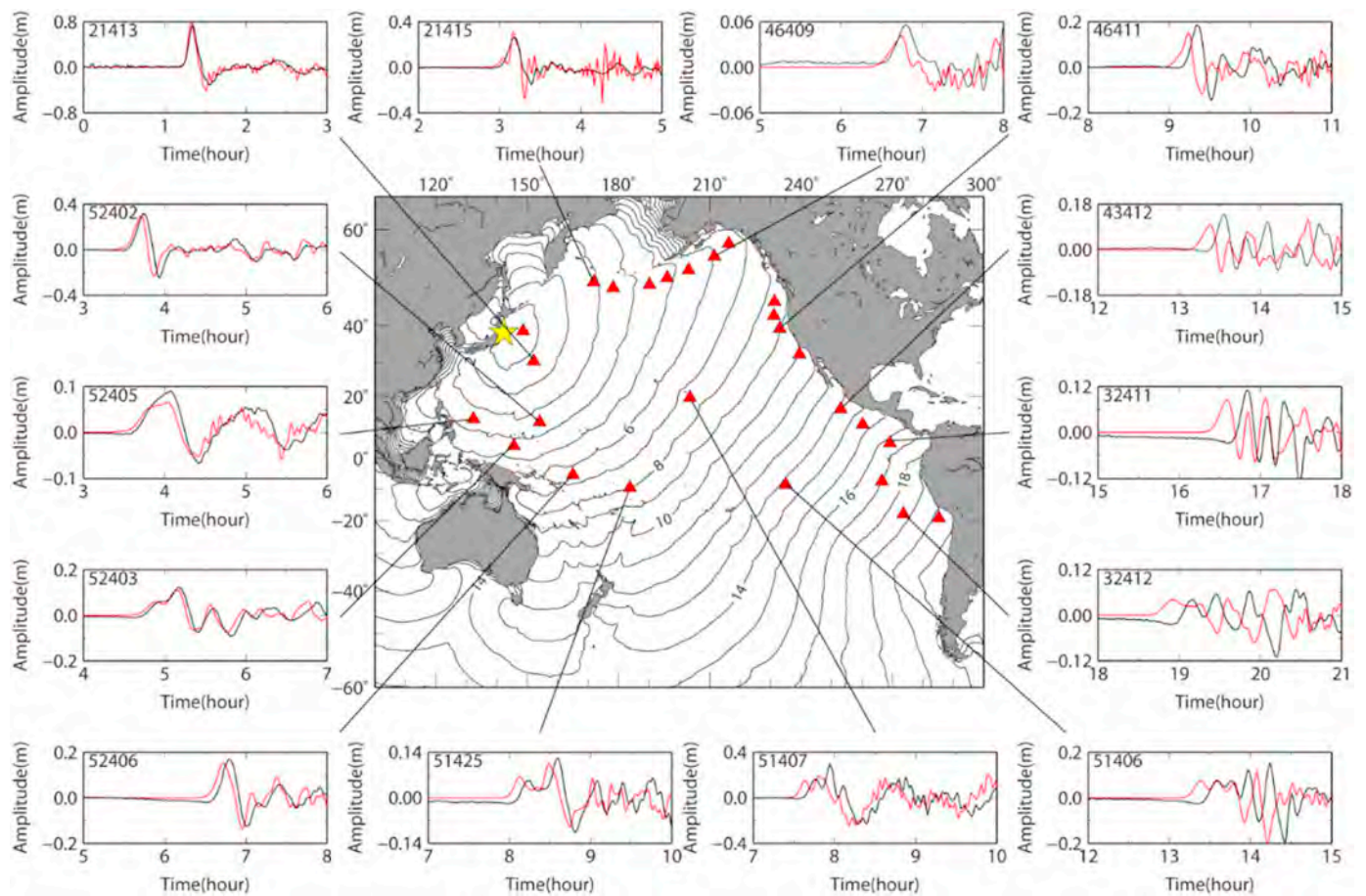


Fig. 7. Computed tsunami travel times (contours) from the 2011 Tohoku earthquake (yellow star). The observed (black) and simulated (red) tsunami waveforms at DART bottom pressure gauges (locations are shown by red triangles) are shown. Based on Watada et al. (2014). (For interpretation of the references to colour in this figure legend, the reader is referred to the web version of this article.)

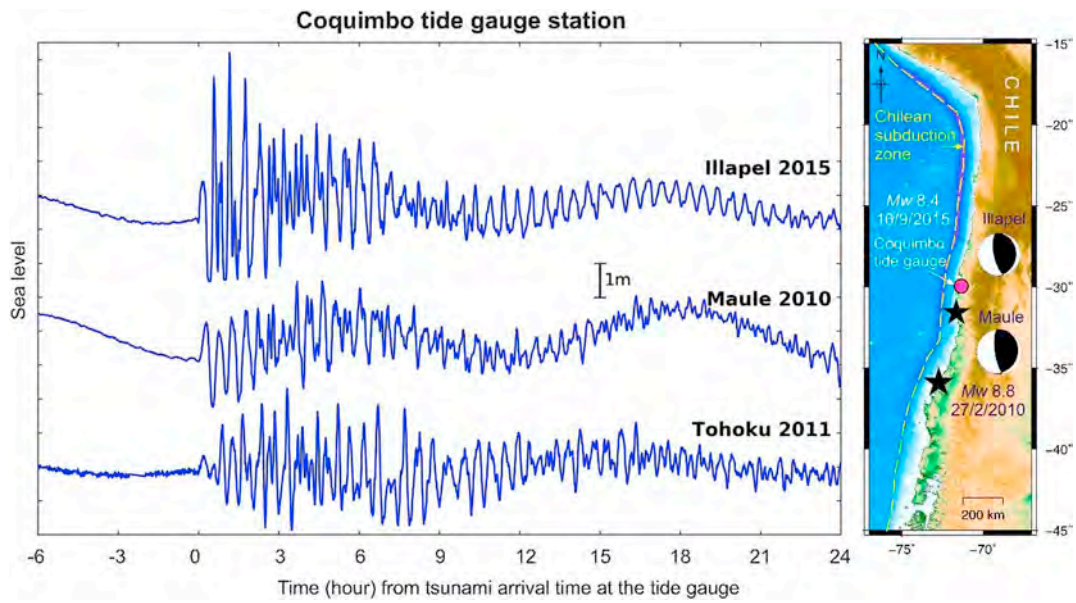


Fig. 8. Observed tsunami waveform at Coquimbo tide gauge station from the 2015 Illapel, 2010 Maule, and 2011 Tohoku earthquakes (see right map for their locations). Time axis is aligned with the tsunami arrival time.

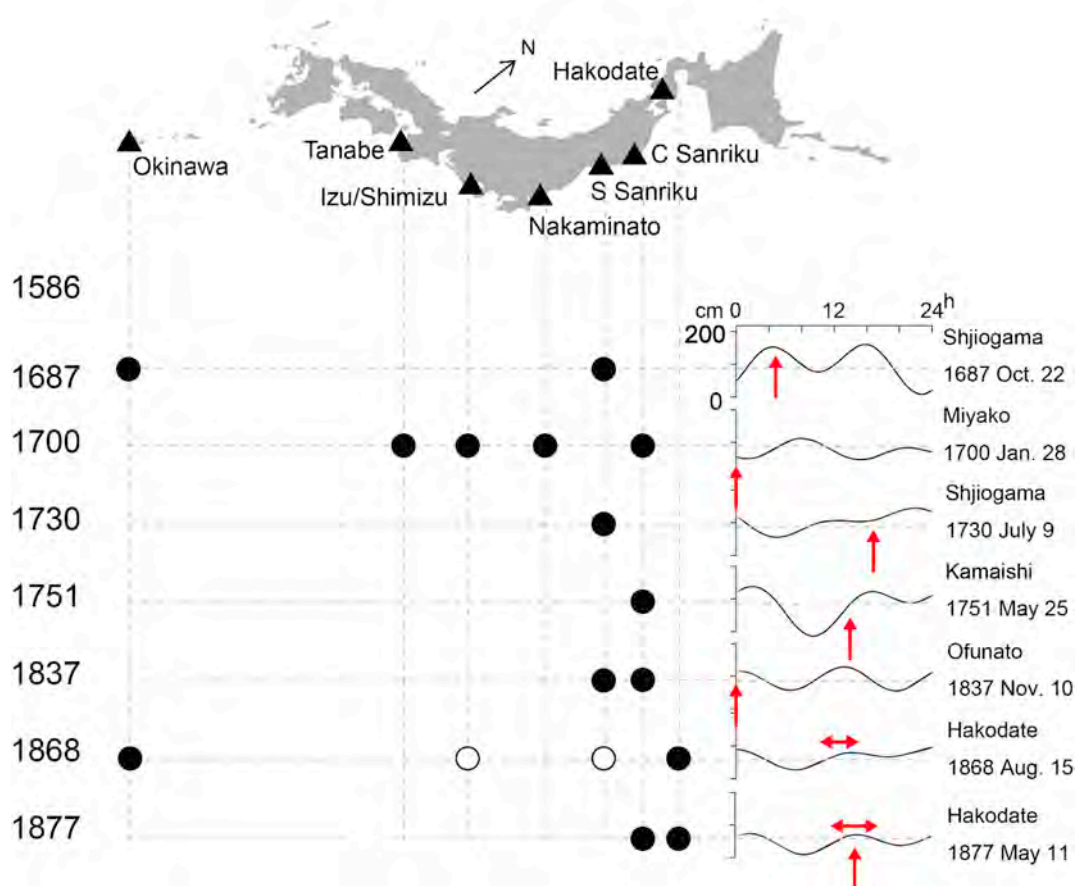


Fig. 9. The summary map of tsunamis recorded in Japan from earthquakes in Cascadia, Peru and Chile. Solid circles indicate tsunamis documented in contemporary documents. Open circles are the tsunami descriptions without original or contemporary documents. Tide levels above Nearly Lowest Low-Water Level (zero level on the vertical axis) are computed at the location and on the days (Japan Standard Time) given in the right, using the program on website of Japan Coast Guard https://www1.kaiho.mlit.go.jp/JODC/marine/umi/tide_pred.html. Mean sea level at each port is shown in gray dashed line. The red arrows indicate the documented tsunami arrival time (vertical arrows for exact time and horizontal arrows for the time range). (For interpretation of the references to colour in this figure legend, the reader is referred to the web version of this article.)

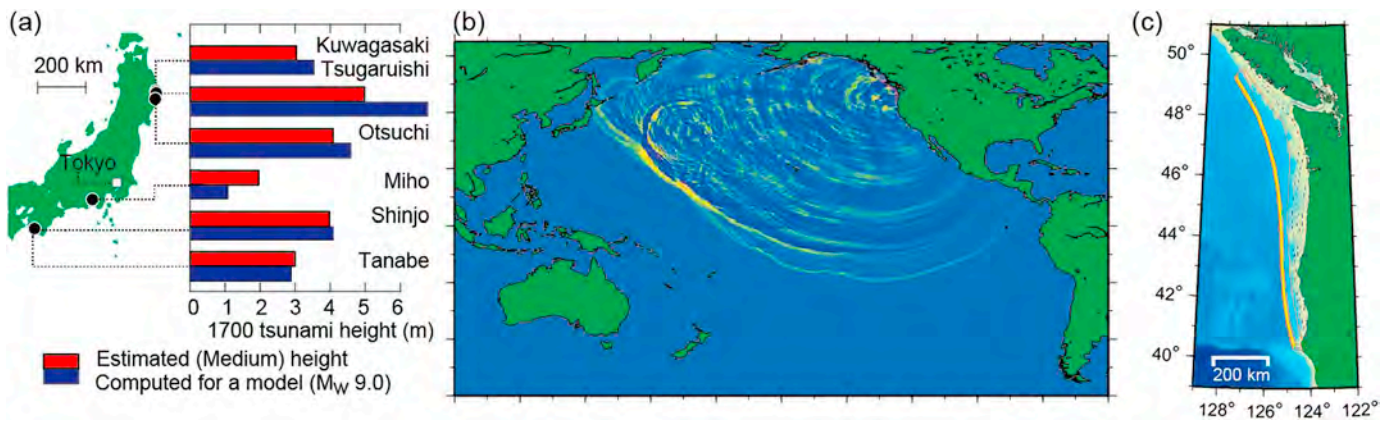


Fig. 10. (a) Comparison of estimated and computed tsunami heights at six locations in Japan. (b) Snapshot of tsunami propagation. (c) Crustal displacement computed based on a fault model in Cascadia subduction zone. Data from Satake et al. (2003).

Tsunamis from some of these earthquakes were recorded in Japan. Tsuji (2013) summarized the historical tsunamis from Chile and Peru subduction zones recorded in Japan. We re-examined the original documents and describe them below, with computed tides (Fig. 9).

The 1730 earthquake off Valparaiso is considered to be the largest one in central Chile (Carvajal et al., 2017b). Official record of Date clan

(presently Miyagi prefecture, Japan) reported that the tsunami arrived at ~ 5 pm on July 9 at Shioagama, without causing damage, but caused damage in salt fields in Ofunato and Akasaki. At that time, the tide level started to rise from the mean sea level (Fig. 9). Another document on Date clan, compiled in 1915, described that the tsunami damaged barriers and rice paddies in Miyagi, Ojika, Monou, and Motoyoshi

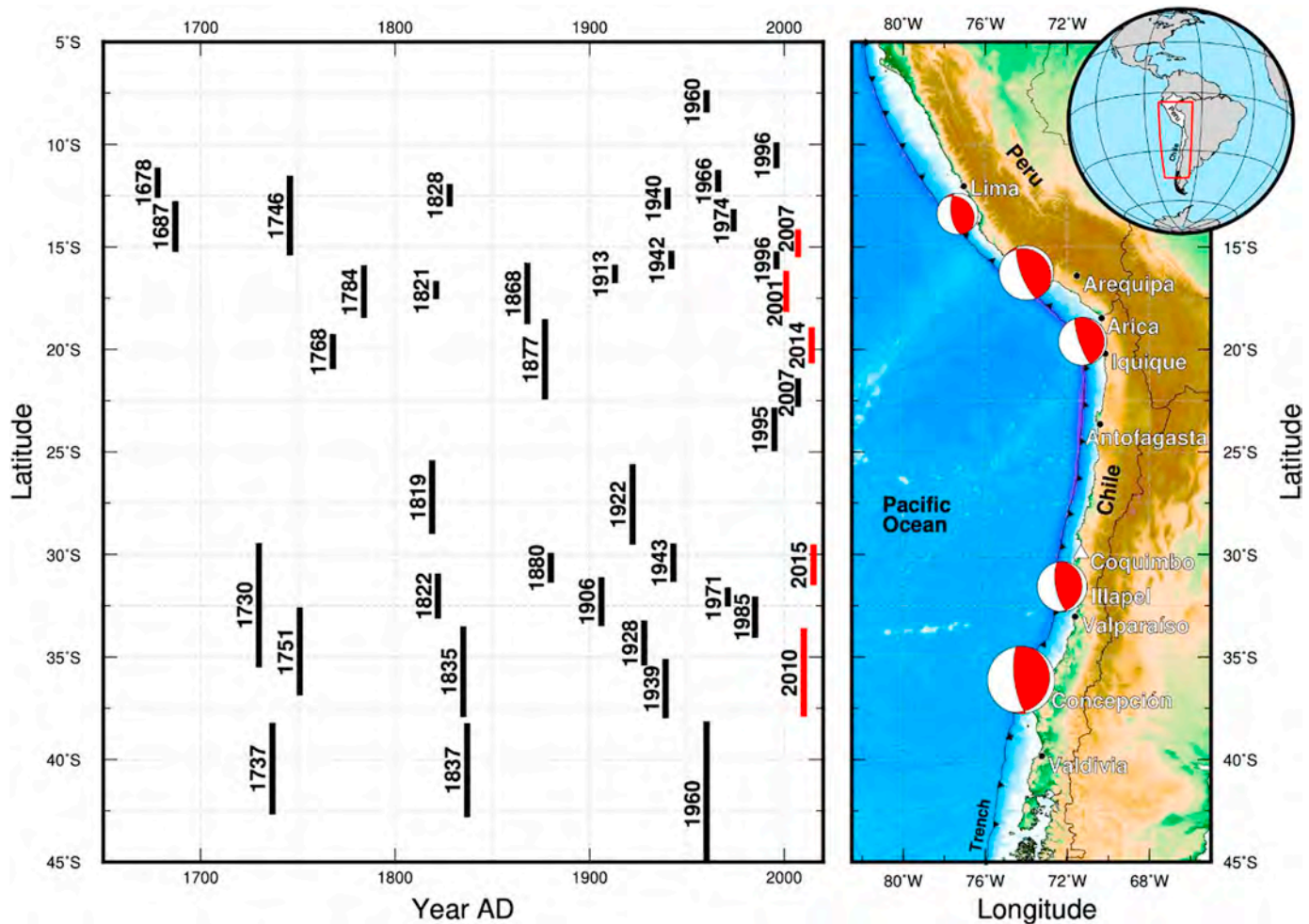


Fig. 11. Focal mechanism solutions (red beach balls) of Global CMT project for recent great ($M_w \sim 8$) earthquakes off Peru and Chile (2001 and 2007 Peru, 2014 Maule, 2014 Iquique, and 2015 Illapel earthquakes). Source zones of recent and historical earthquakes are shown in red and black bars, respectively, at corresponding latitude (Kelleher, 1972; Comte and Pardo, 1991; Beck et al., 1998; Schurr et al., 2014). Location of Coquimbo tide gauge station, where the tsunami waveforms in Fig. 8 are recorded, are shown by white triangle. (For interpretation of the references to colour in this figure legend, the reader is referred to the web version of this article.)

counties. Tsuji (2013) estimated the tsunami height at ~ 2 m in these locations. Carvajal et al. (2017b) compared these heights with those from the 1960 earthquake (Mw 9.5, tsunami heights 2–5.5 m) and the 2010 Maule earthquake (Mw 8.8, the heights are less than 2 m), and estimated the 1730 earthquake size at Mw = 9.1–9.3.

The 1751 earthquake off Concepcion may have occurred in the same region as the 2010 Maule earthquake (Fig. 11). One document in Otsubuchi town, on the Sanriku coast, reported, on May 25: “at around 2 pm, a series of tides, seven times of high tide and five times of low tide, flooded the floor of houses, and submerged rice paddies and fields.” It ended around 6 pm, and caused no injury to humans or horses.” The tide level was higher than the mean sea level, during the above time period (Fig. 9). Tsuji (2013) also attributed another document to the 1751 tsunami, which described tsunamis in Ojika, Monou, Motoyoshi, and Kesen counties, but the date was July 24, approximately two months later.

The 1837 earthquake occurred in the same region as the 1960 giant earthquake (Mw 9.5) off Valdivia, but with a smaller size (Fig. 11). The tsunami reached Japan and damaged rice paddies in Miyagi, Ojika, Motoyoshi, and Kesen counties, according to two official records of Date clan. The tsunami arrived around midnight of November 8 and damaged fishing and salt production facilities in Kesen, Akasaki, and Ofunato, surprised residents in Onagawa and Kamaishi, according to three independent local documents. They all emphasized that the tsunami came without an earthquake. The tide level was the highest around midnight (Fig. 9).

The 1877 earthquake (Mw 8.9) off Iquique (then Peru) occurred on May 9. The tsunami was observed at many places in the Pacific (Milne, 1880; Honda et al., 1908). In Hawaii, the tsunami arrived at 4:45 am, with height of 12 m, and continued for a day in Hilo, and was observed at six other locations with smaller heights. The tsunami height was 4 m in Samoa Islands. The tsunami arrived in New Zealand at ~ 7 am, 1–3 m high, at many places. In Japan, the tsunami appeared in Kamaishi at ~ 9 –10 am, and the period was ~ 15 min at around noon, with the maximum height of ~ 2 m above high tide level. In Hakodate, the sea receded at 11:30 am, then rose 2 m with a period of 20 min. The maximum tsunami, with a height of 2.4 m, overflowed the town (Hakodate) at $\sim 2:30$ pm. This time corresponds to the highest tide of that day, but it was around the mean sea level (Fig. 9). The large wave invaded Kazusa in Chiba prefecture around noon, and a consequent wave devastated the coast at 4 pm, causing the loss of many lives (Honda et al., 1908).

3.3. Tsunamis from historical earthquakes in Peru

Great earthquakes in Peru subduction zone and corresponding tsunami have been documented (e.g., Dorbath et al., 1990). Great earthquakes occurred in 1586 and 1687 off Central Peru (Fig. 11), and their magnitudes were estimated at Mw 8.1 and 8.4, respectively (Villegas-Lanza et al., 2016).

The 1586 earthquake was the oldest earthquake that damaged Lima; Dorbath et al. (1990) estimated the tsunami height in Callao at 5 m. The tsunami heights in Japan had been estimated to be between 2.0 and 2.5 m (e.g., in NOAA database). Okal et al. (2006) could not make a source model to explain tsunami heights in both Callao and Japan. We found that the Japanese tsunami record was erroneously created; hence, the 1586 tsunami in Japan should be dismissed for a few reasons: first, there is no written document of the 1586 tsunami (Tsuji, 2013). Soon after the 1960 tsunami from Chile, Ninomiya (1960) compiled historical tsunami records on the Sanriku coast, and correlated a tsunami legend in Tokura village with the 1586 Peru earthquake, although he noted that the dates were different. Regarding the legend, Kunitomi (1933), during the compilation of historical tsunami data following the 1933 Sanriku tsunami, referred to a tsunami history book of Miyagi prefecture, published in 1903, after the 1896 Meiji Sanriku tsunami. It described that the tsunami legend was in Tensho

13th year, 5th month and 14th day on the Japanese calendar, or June 11, 1585 on the Gregorian calendar. There was an earthquake and possibly tsunami damage in central Japan, in the same year (Tensho 13th year), on the Japanese calendar. However, the latter date is January 18, 1586 on the Gregorian calendar, and the legend date was erroneously changed to 1586, which was the same year of the Peru earthquake (Hayashi et al., 2018). Following the 2011 Tohoku tsunami, the tsunami legend in Tokura was studied again (Ebina, 2015). A local person published a story he heard from his grandfather that many small valleys were named following the 1611 tsunami, which inundated further inland than the 2011 tsunami. Ebina (2015), based on other historical documents, concluded that the legend existed around 1750. This may correspond to the above legend for the 1586 tsunami, although the year was different. Therefore, we conclude here that the tsunami legend in Tokura is unlikely to be linked to the 1586 Peruvian earthquake.

The tsunami height from the 1687 earthquake was estimated at 5 to 10 m, on the Peruvian coasts (Dorbath et al., 1990) and was documented in two locations in Japan. In Shiogama, the official Date clan records noted that the sea started to rise and fall around 5 am, on October 22, with amplitude of ~ 0.5 m. It continued 12 times until 7 pm, indicating that the tsunami period was ~ 1 h. The tsunami arrived during high tide, when the sea level was ~ 1 m higher than the mean sea level (Fig. 9); hence, the tsunami with a 0.5 m amplitude would have been clearly noticed. Such disturbance lasted three days. Another official record from Ryukyu kingdom reported that in Yonagusuku county (central part of Okinawa Island), the sea rose and fell three times, starting at 2 am on October 21 with an amplitude of 80% of tide (0.8 m), and repeated 3 to 4 times.

Tsunamis from the 1868 Arica earthquake (Mw 8.8), the largest event in southern Peru, were also recorded around the Pacific Ocean (Milne, 1880; Honda et al., 1908). Captain Blakiston made account for the Hakodate port reporting: “On August 15 at 10:30 am, a series of bores or tidal waves commenced and lasted until 3 pm. In ten minutes, there was a difference in the sea level of 10 feet, the water rising above high water and falling below low water mark with greater rapidity.” This time period corresponds to the high tide of the day, although the sea level was around the mean sea level (Fig. 9). The Ryukyu kingdom record documented that in Naha port of Okinawa Island the unusual tide level change repeated 16 to 17 times, from 8 am to 10 pm on August 15. The tsunami reports in Motoyoshi (Miyagi prefecture) and Shimoda (JMA, 1961; Tsuji, 2013) are not reported in contemporary documents; thus, they could be questionable. At the Sandwich Islands, the sea oscillation, with 10 min intervals, continued for three days. At Chatham Island near New Zealand, the tsunami height was 10 m, and caused a few casualties. This was the only tsunami casualty in New Zealand (Power, 2013). On the main islands of the New Zealand, tsunami height was 1 to 4 m.

4. Modeling trans-oceanic tsunamis

In this section, we briefly review various methods to quantify the trans-oceanic tsunamis. The tsunami magnitude scale relates the tsunami heights and the earthquake size. Tsunami travel times can be computed from actual bathymetry, and the ray tracing provides relative tsunami amplitudes, due to focusing/defocusing caused by bathymetry. Tsunami numerical simulation, starting from seafloor displacement computed from fault models, produces tsunami amplitudes and waveforms, and indicates strong directivity due to strike of fault or subduction zones. Far-field tsunamis are often long-lasting, due to multiple reflections or resonance at bays/harbors.

4.1. Tsunami magnitude

The tsunami magnitude scale, M_t , was defined and used for numerous earthquakes (Abe, 1979). The definition of M_t for a trans-

Pacific tsunami is:

$$Mt = \log H + C + 9.1$$

where H is the maximum amplitude recorded on the tide gauges in meters, and C is the distance factor, ranging from -0.6 to $+0.3$, depending on a combination of the source and the observation points. For an earthquake in Peru or Chile and observation points in Japan, $C = 0.0$. The above formula was calibrated with the moment magnitude scale (M_w) of the earthquakes; hence, the tsunami height (H) can be predicted using the above formula if the moment magnitude of the earthquake is known. For an earthquake in Peru or Chile with $M_w = 9.1$, the tsunami amplitude (H) in Japan would be 1 m, and it would be 2.5 m for an earthquake with $M_w = 9.5$. We note that the empirical relation derived from recent Chilean tsunami amplitudes recorded in Japan and the moment magnitude derived by Carvajal et al. (2017a), described in Section 2.4, was similar to the above tsunami magnitude formula.

4.2. Tsunami travel time and ray tracing

For hydrodynamic computation of tsunami propagation and coastal amplification, if the horizontal scale of motion (wavelength) is much larger than the water depth, the shallow-water wave (or long wave) theory can be adopted. Typical ocean depth is $\sim 4\text{--}5$ km, while a large earthquake has a source area of several tens to hundreds of kilometers; hence, the long-wave approximation is appropriate for earthquake-generated tsunamis. In addition, for water depth larger than ~ 50 m, nonlinear effects such as advection or bottom friction can be ignored, and the linear long-wave theory can be used, which gives tsunami velocity (c) as $c = \sqrt{gd}$, where g is gravitational acceleration (9.8 m/s^2) and d is water depth. For most paths of tsunami propagation, except near the coast, the linear long wave theory is valid; hence tsunami travel time can be computed if the ocean depth along the tsunami propagation path is known.

The tsunami propagation or travel time can be represented by their wavefront at each time, on the basis of the Huygens' principle. Once the tsunami source is specified, travel time can be computed and presented as travel time (or refraction) diagram (Figs. 2, 3, 6 and 7). This diagram does not provide information on the tsunami amplitude.

The tsunami propagation can also be expressed in terms of tsunami rays, which are perpendicular to the tsunami wavefront. Tsunami ray tracing represents focusing and defocusing of rays, thus revealing relative amplitude of tsunamis as they propagate across the ocean (Satake, 1988). Fig. 12 shows an overview of the spread of tsunamis from sources generated in different subduction zones in the Pacific Ocean. Tsunami ray tracing from a source off Chile, assuming a uniform water depth (Fig. 12a left) shows that the tsunami rays are radiated uniformly from the source; the rays spread up to around Hawaii, then concentrate towards Japan. This is because of the sphericity of the Earth. Waves propagate on a sphere spread until angular distance of 90° , then start to converge towards the antipode (the opposite point of the Earth, or angular distance of 180°). The angular distance between Chile and Japan is $\sim 150^\circ$; hence, the rays show a converging pattern even for a uniform water depth. The reciprocity between events generated in Chile (Fig. 12a) and Japan (Fig. 12e) is clear. The ray tracing for actual bathymetry (Fig. 12a right) indicates that the rays originated from Chile are refracted at East Pacific rise, and are concentrated towards Japan. For a Peruvian source (Fig. 12b), the convergence pattern of the rays shows that propagation of the tsunami is favored towards Taiwan and northeastern Philippines. For events generated in Alaska (Fig. 12c), the rays demonstrate concentration towards northwestern Oceania and Chile. Tsunamis from the Aleutian Islands (Fig. 12d) are channeled towards several destinations in the Pacific Ocean, including the southeast area of Asia, northeastern Oceania, and south-central Chile.

For recent trans-Pacific tsunamis, such as the 2010 Chile tsunami or

the 2011 Tohoku tsunami, discrepancies in travel time (a few percent of total travel time), between observed waveforms recorded by offshore tsunami gauges (DART bottom pressure gauges) and the computations based on linear long-wave theory, have been reported (see Fig. 7). This delay is due to the smaller phase velocity for real tsunami waves than that predicted by simulations based on linear long-waves, due to the coupling of elastic Earth and water. When the effects of elasticity of Earth and sea water, as well as gravitational potential and sea water stratification, are taken into account for tsunami simulations, the travel time delay becomes much smaller (Watada et al., 2014; Ho et al., 2017).

4.3. Tsunami numerical computations and directivity

For computation of tsunami amplitudes or waveforms, the finite-difference method has been popularly adopted to directly solve the equations of motion and continuity for linear or nonlinear shallow water equations (Shuto, 1991; Satake, 2015a). Seafloor displacement, due to faulting, is computed from nine static fault parameters (i.e., longitude, latitude, depth, strike angle, dip angle, rake angle, length, width, and slip amount) (Okada, 1985) that are used as the initial condition (or initial sea surface displacement) for tsunami simulations.

Fig. 13 compares the maximum sea surface height distribution from four fault models, off west USA (Cascadia), Alaska, Peru, and Chile. The Cascadia fault has a length and a width of 1050 km and 90 km respectively, and uniform slip of 14 m, based on the model of the 1700 Cascadia earthquake (Satake et al., 2003). The respective values for Alaska fault are 1200 km, 90 km, and 14 m, based on the model of the 1964 Alaska earthquake. The M_w for the two earthquakes is in the range of 9.0–9.1. The fault models for Peru (a 1687 earthquake model) and Chile (a 2010 Maule earthquake model) have the same size ($300 \text{ km} \times 150 \text{ km}$) and slip amount (10 m); hence, the moment magnitudes (M_w 8.8) are the same. The M_9 earthquake off Cascadia directs most of its far-field tsunami energy towards Japan, Philippines, and east Indonesia, whereas the M_w 9 source in Alaska mostly affects South American coasts (e.g., Peru, Chile) in the far-field. The source off Peru shows that the far-field tsunami energy is focused towards southwest (e.g., New Zealand), while the source off Chile shows the far-field energy is mainly focused towards northwest (e.g., Japan).

The main difference in the fault models is the strike direction of the fault, which is parallel to the subduction zones. The strike angle for the earthquake in Cascadia is SE-NW, while it is SW-NE for Alaska. The subduction zone orientation is NW-SE off Peru, while it is roughly N-S (NNE – SSW) off Chile. The tsunami energy is the largest in the direction perpendicular to the strike direction. This is known as the radiation pattern, often called as the directivity of tsunamis (Ben-Menahem and Rosenman, 1972). The historical facts that the tsunamis from Chile earthquakes (e.g., the 1960 earthquake) were large in Japan, while the tsunami from the Peru earthquake (e.g., 1868 Arica earthquake) was large in New Zealand, can be explained by the directivity effect.

4.4. Duration of tsunamis

Tsunami waveforms, particularly the duration and appearance time of maximum amplitudes after the first arrival, vary significantly from one tsunami to another. Watanabe (1972) classified the tsunami waveforms on tide gauges into three types. The “A” type shows one or a few large waves near the first arrival (e.g., the Illapel tsunami at Coquimbo in Fig. 8), and occurs mostly at isolated islands in the Pacific Ocean and occasionally at continental coasts. The “B” type tsunami record consists of one or a few wave groups (e.g., the 2010 Maule or 2011 Tohoku tsunamis in Coquimbo; Fig. 8), and is mostly distributed on the continental coast and along the island-arc. The “C” type is a combination of the “A” and “B” types and the distribution differs from one tsunami to another.

Tsunami waveforms from trans-oceanic tsunamis often show long-

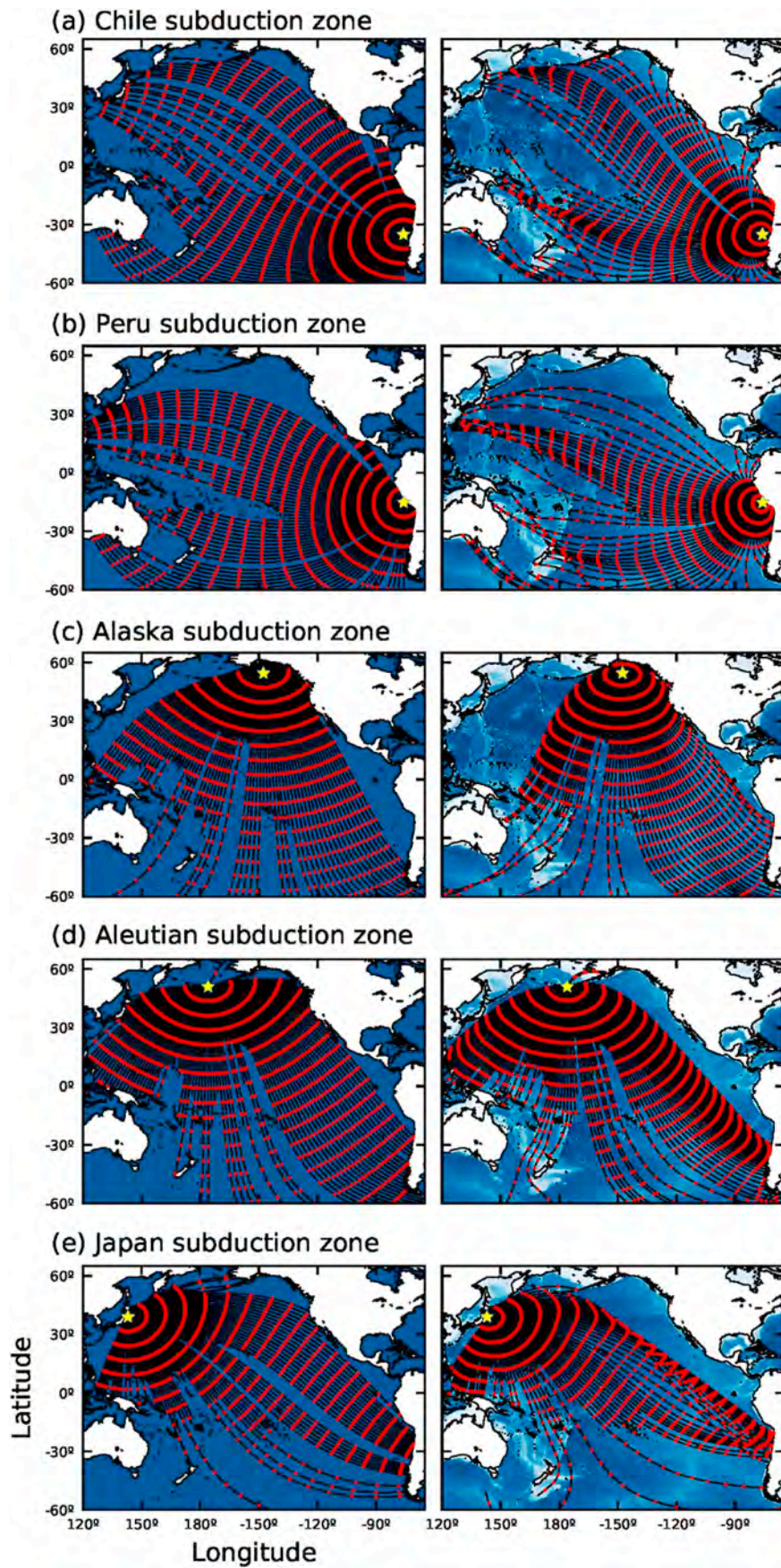


Fig. 12. Ray tracing for sources located around the Pacific Ocean computed for a uniform (5400 m) depth (left) and actual ocean bathymetry (right). Each tick is one hour from the origin time. Based on Satake (1988).

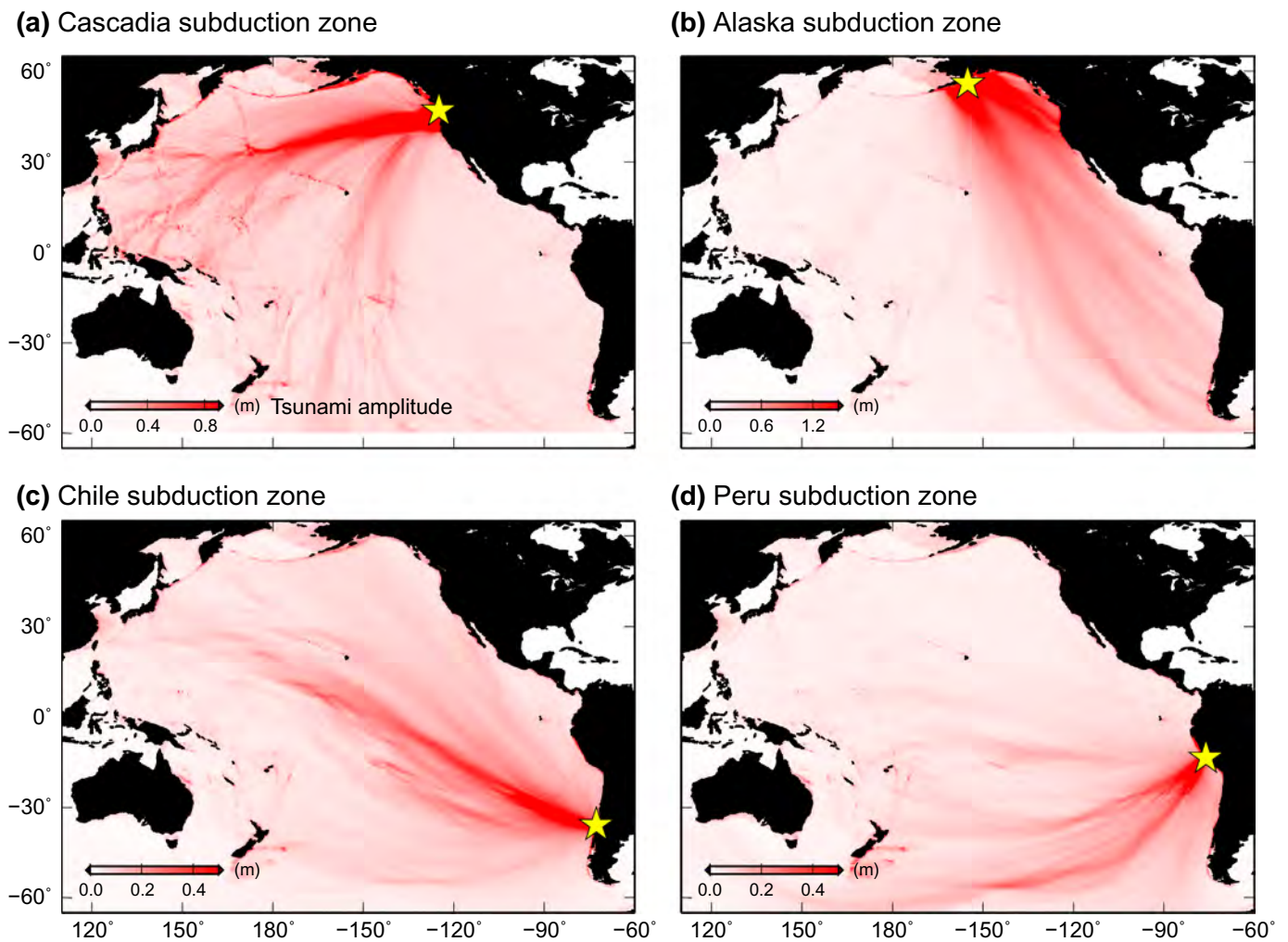


Fig. 13. Maximum tsunami amplitudes for a source in Cascadia subduction zone, offshore west coast of USA (a), Alaska (b), Chile (c), and Peru (d). For Cascadia, the fault has a length and a width of 1050 km and 90 km, respectively, and uniform slip of 14 m. The respective values for Alaska are 1200 km, 90 km, and 14 m. For the two cases of Peru and Chile, 300 km long and 150 km wide fault with 10 m slip were used for the initial conditions.

lasting waves (B or C types in Watanabe's classification) because of multiple reflections of tsunamis across the basin (Saito et al., 2013) or multiple reflections on continental shelf (González et al., 1995; Yamazaki and Cheung, 2011; Fujii and Satake, 2013). In addition, they have very long (40 to 100 min) predominant periods, because of the huge size of tsunami source (Heidarzadeh and Satake, 2014) and the resonance at local bays (Abe, 2000). For the 2011 Tohoku tsunami, the tsunami traveled across the Pacific Ocean and was reflected back from the South American coast; the reflected waves were detected ~ 48 h after the earthquake at some offshore bottom pressure gauges (Saito et al., 2013). The long-lasting waves at Coquimbo from the 2011 Tohoku tsunami may represent multiple reflections of the incoming wave on the continental shelf.

Edge waves are waves slowly travelling along the coast, with amplitudes decaying with offshore distance. The tsunami energy is trapped on continental shelves near the source and might produce late maximum amplitudes from positive interference of secondary tsunami waves (B type), creating a pattern of quasi-stationary standing nodes and antinodes along the coast (e.g., during the 2010 Maule earthquake; Yamazaki and Cheung, 2011). The tsunami waveforms at Coquimbo from the 2010 Maule earthquake represent such edge waves (see Fig. 8).

For resonance at bays/harbors, the fundamental oscillation mode (T_c) for a one-dimensional rectangular bay with a length of L and a

constant water depth of d is given as $T_c = 4L/\sqrt{gd}$ (Honda et al., 1908). For the case of Miyako bay (see Section 2.4) we have: $L = 10$ km, $d = 20$ m; hence the fundamental mode becomes $T_c = 48$ min, which is the dominant period of later waves of the 1960 tsunami in the Miyako Bay (see Fig. 5). If a wave approaching the bay has such a long-period component, then the resonance mode of the bay will be excited, explaining the long-duration of oscillations within the bay. The resonant mechanism in combination with local bathymetric features (e.g., focusing) may result in the amplification of tsunami amplitudes, from the entrance of the bay to the innermost part of the embayment, in a way similar to tidal amplification from resonance at longer periods (e.g., Garrett, 1972). This effect might explain some local tsunami wave amplification during the 1960 Chile tsunami in Japan (see Section 2.4, Fig. 5).

These mechanisms, including trapped energy by edge waves near the source, multiple reflections across the basin or on continental shelf, or resonance at embayments, are within the framework of long-wave (shallow-water) simulations on actual topography/bathymetry. Thus, numerical computations of tsunamis on actual bathymetry includes such effects, as long as the grid resolution is fine enough to include the bathymetric features, particularly for bays and harbors. For example, to accurately model tsunami effects in ports and bays, a grid resolution of ~ 50–100 m is required.

5. Concluding remarks: Implication to paleo-tsunami studies

We have reviewed past trans-oceanic tsunamis recorded instrumentally or documented historically, and examined their characteristics. We now discuss their implications to paleo-tsunami studies. As we have seen in historical cases (Section 2), a giant ($M_w \sim 9$) earthquake usually generates trans-oceanic tsunamis. The tsunami magnitude formula (Section 4.1) indicates that the earthquake size must be $M_w > 9$ for a tsunami amplitude of > 1 m across the Pacific Ocean. Smaller tsunamis can be detected instrumentally, as we have seen in Section 2, but if their amplitudes are within the range of ocean tide, the tsunami may not cause damage or move sediments to be deposited; hence, it would be difficult to be recorded in historical documents or coastal geological layers.

Giant earthquakes with $M_w > 9$ are rare phenomena; only five events are known in the last century (Satake and Atwater, 2007). Although statistical studies on current seismicity in global subduction zones have concluded that the long-term average would be lower, i.e., 1–3 events per century (McCaffrey, 2008), recent studies support the former estimate (i.e., five $M_w \sim 9$ earthquakes in a century) (Kagan and Jackson, 2013). These studies indicate that instrumental seismological data are too few to cover the recurrence period of such giant ($M_w \sim 9$) earthquakes, and that $M_w 9$ events can occur in any subduction zone. Further, Rong et al. (2014) concluded that most subduction zones around the Pacific Ocean can generate $M_w > 8.5$ earthquake with an average recurrence of 250 years, and $M_w > 9.0$ event can be expected within a sufficient time period ($\sim 10,000$ years). Therefore, if the coastal geological layers cover a long and continuous period, deposits by trans-oceanic tsunamis, from subduction zones different than the ones that historically produced the tsunamis, may be preserved.

Directivity effect (Section 4.3) is an important factor to control the tsunami amplitude, and the effects can be evaluated by consideration of tectonics of the tsunami source and numerical computation of tsunami generation and propagation. Hence, the geometrical relations between the target subduction zones and tsunami deposit study sites need to be examined (Fig. 13). For example, an $M_w 9$ source in Alaska would be expected to leave most tsunami deposits in Peru and Chile rather than in Japan (Fig. 13b). Similarly, a $M_w 9$ source in Cascadia would produce probably thicker tsunami deposit layer in Japan or in Western Pacific Ocean rather than in Peru (Fig. 13a). Therefore, in case of looking for far-field tsunami deposits from large earthquakes in Cascadia, it is recommended to look for them in Japan or in the western Pacific.

Another unique feature of the trans-oceanic tsunamis is the long duration with multiple waves, due to multiple-reflections and oscillation at bays. The waveforms of trans-oceanic tsunamis are different from those of nearby earthquakes, which are characterized by single maximum peak at first arrival. Such a difference may be affected by local condition, such as resonance at the embayment scale, and may influence the tsunami deposits. Multiple-bed deposits, composed of a stack of several sharp-based and graded layers, are attributed to repeated alternation of current directions and interpreted to have been caused by long-lasting tsunamis with large amplitude in the middle stage (Fujiwara, 2008); hence, they may represent trans-oceanic tsunamis.

Declaration of Competing Interest

The authors declare that they have no known competing financial interests or personal relationships that could have appeared to influence the work reported in this paper.

Acknowledgements

We thank Prof. K. Goto for providing us an opportunity to write this review paper, and two anonymous reviewers for their many valuable

comments that improved the paper. This work was supported by JSPS KAKENHI Grant JP16H01838. MH was funded by the Royal Society (grant number CHL/R1/180173) and the Japan Society for the Promotion of Science (JSPS) (grant number JSPS/IP/19003).

References

- Abe, K., 1979. Size of great earthquakes of 1873–1974 inferred from tsunami data. *J. Geophys. Res.* 84, 1561–1568. <https://doi.org/10.1029/JB084iB04p01561>.
- Abe, Ku., 2000. Predominance of long periods in large Pacific tsunamis. *Sci. Tsunami Hazards* 18, 15–34. <https://library.lanl.gov/tsunami/ts181.pdf>.
- Atwater, B.F., Musumi-Rokkaku, S., Satake, K., Tsuji, Y., Ueda, K., Yamaguchi, D.K., 2015. The orphan tsunami of 1700—Japanese clues to a parent earthquake in North America. In: U. S. G. S. Professional Paper 1707, 2nd ed. pp. 135. <https://doi.org/10.3133/pp1707>.
- Bache, A.D., 1856. Notice of earthquake waves on the western coast of the United States, on the 23d and 25th of December, 1854. *Am. J. Sci. Arts* 21, 37–43. <https://www.biodiversitylibrary.org/item/92736#page/1/mode/1up>.
- Beck, S., Barrientos, S., Kausel, E., Reyes, M., 1998. Source characteristics of historic earthquakes along the Central Chile subduction zone. *J. S. Am. Earth Sci.* 11, 115–129. [https://doi.org/10.1016/S0895-9811\(98\)00005-4](https://doi.org/10.1016/S0895-9811(98)00005-4).
- Ben-Menahem, A., Rosenman, M., 1972. Amplitude patterns of tsunami waves from submarine earthquakes. *J. Geophys. Res.* 77, 3097–3128. <https://doi.org/10.1029/JB077i017p03097>.
- Berkman, S.C., Symons, J.M., 1964. The Tsunami of May 22, 1960 as Recorded at Tide Stations. U.S. Department of Commerce, Coast and Geodetic Survey, pp. 79.
- Butler, R., Burney, D.A., Rubin, K.H., Walsh, D., 2017. The orphan Sanriku tsunami of 1586: new evidence from coral dating on Kaua'i. *Nat. Hazards* 88, 797–819. <https://doi.org/10.1007/s11069-017-2902-7>.
- Carvajal, M., Cisternas, M., Gubler, A., Catalán, P.A., Winckler, P., Wesson, R.L., 2017a. Reexamination of the magnitudes for the 1906 and 1922 Chilean earthquakes using Japanese tsunami amplitudes: Implications for source depth constraints. *J. Geophys. Res.* 122, 4–17. <https://doi.org/10.1002/2016JB013269>.
- Carvajal, M., Cisternas, M., Catalán, P.A., 2017b. Source of the 1730 Chilean earthquake from historical records: Implications for the future tsunami hazard on the coast of Metropolitan Chile. *J. Geophys. Res.* 122, 3648–3660. <https://doi.org/10.1002/2017JB014063>.
- Chagué-Goff, C., Goff, J., Nichol, S.L., Dudley, W., Zawadzki, A., Bennett, J.W., Mooney, S.D., Fierro, D., Heijnis, H., Dominey-Howes, D., Courtney, C., 2012. Multi-proxy evidence for trans-Pacific tsunamis in the Hawaiian Islands. *Mar. Geol.* 299–302, 77–89. <https://doi.org/10.1016/j.margeo.2011.12.010>.
- Choi, B.H., Pelinovsky, E., Kim, K.O., Lee, J.S., 2003. Simulation of the trans-oceanic tsunami propagation due to the 1883 Krakatau volcanic eruption. *Nat. Hazards Earth Syst. Sci.* 3, 321–332. <https://doi.org/10.5194/nhess-3-321-2003>.
- Comte, D., Pardo, M., 1991. Reappraisal of great historical earthquakes in the northern Chile and southern Peru seismic gaps. *Nat. Hazards* 4, 23–44. <https://doi.org/10.1007/BF00126557>.
- Dorbath, L., Cisternas, A., Dorbath, C., 1990. Assessment of the size of large and great historical earthquakes in Peru. *Bull. Seismol. Soc. Am.* 80, 551–576. <https://pubs.geoscienceworld.org/ssa/bssa/article-standard/80/3/551/119293/assessment-of-the-size-of-large-and-great>.
- Earthquake Research Committee, 2013. Long-term evaluation of seismicity along Nankai Trough (2nd version) (in Japanese). Headquarters for Earthquake Research Promotion, pp. 14. http://www.jishin.go.jp/main/chousa/13may_nankai/index.htm.
- Eaton, J.P., Richter, D.H., Ault, W.U., 1961. The tsunami of May 23, 1960, on the Island of Hawaii. *Bull. Seismol. Soc. Am.* 51, 135–157. <https://pubs.geoscienceworld.org/ssa/bssa/article/51/2/135/116019/the-tsunami-of-may-23-1960-on-the-island-of-hawaii>.
- Ebina, Y., 2015. Analysis of historical documents and the tradition of the historical tsunami in the Tohoku -mainly on the new appearance historical documents about the 1611 Keicho Oshu earthquake and tsunami. *Res. Rep. Tsunami Eng.* 32, 231–239. http://www.tsunami.civil.tohoku.ac.jp/hokusaiz/3/publications/pdf2/vol.32_15.pdf.
- Ewing, M., Press, F., 1955. Tide-gage disturbances from the great eruption of Krakatoa. *Trans. Am. Geophys. Union* 36, 53–60. <https://doi.org/10.1029/TR036i001p00053>.
- Fujii, Y., Satake, K., 2013. Slip distribution and seismic moment of the 2010 and 1960 Chilean earthquakes inferred from tsunami waveforms and coastal geodetic data. *Pure Appl. Geophys.* 170 <https://doi.org/10.1007/s00024-012-0524-2>. 1493–150.
- Fujiwara, O., 2008. Bedforms and sedimentary structures characterizing tsunami deposits. In: Shiki, T., Tsuji, Y., Yamazaki, T., Minoura, K. (Eds.), *Tsunamiites: Features And Implications*, pp. 51–62. <https://doi.org/10.1016/B978-0-444-51552-0.00004-7>.
- Garrett, C., 1972. Tidal resonance in the Bay of Fundy and Gulf of Maine. *Nature* 238, 441–443. <https://doi.org/10.1038/238441a0>.
- González, F.I., Satake, K., Boss, E.F., Mofjeld, H.O., 1995. Edge wave and non-trapped modes of the 25 April 1992 Cape Mendocino tsunami. *Pure Appl. Geophys.* 144, 409–426. <https://doi.org/10.1007/BF00874375>.
- Goto, K., Chavanich, S.A., Imamura, F., Kunthasap, P., Matsui, T., Minoura, K., Sugawara, D., Yanagisawa, H., 2007. Distribution, origin and transport process of boulders transported by the 2004 Indian Ocean tsunami at Pakarang Cape, Thailand. *Sediment. Geol.* 202, 821–837. <https://doi.org/10.1016/j.sedgeo.2007.09.004>.
- Green, C.K., 1946. Seismic sea wave of April 1, 1946, as recorded on tide gages. *Eos Trans. AGU* 27, 490–500. <https://doi.org/10.1029/TR027i004p00490>.
- Gusman, A.R., Murotani, S., Satake, K., Heidarzadeh, M., Gunawan, E., Watada, S.,

- Schurr, B., 2015. Fault slip distribution of the 2014 Iquique, Chile, earthquake estimated from ocean-wide tsunami waveforms and GPS data. *Geophys. Res. Lett.* 42, 1053–1060. <https://doi.org/10.1002/2014GL062604>.
- Hanson, J.A., Reasoner, C.L., Bowman, J.R., 2007. High-Frequency Tsunami Signals of the Great Indonesian Earthquakes of 26 December 2004 and 28 March 2005. *Bull. Seismol. Soc. Am.* 97, S232–S248. <https://doi.org/10.1785/0120050607>.
- Hayashi, Y., Kiyomoto, M., Tange, G., Nishimae, Y., 2018. Negative effects of erroneous records of Japanese tsunami caused by the 1586 earthquake off the coast of Peru being included in the Technical Reports of the Japan Meteorological Agency [in Japanese]. *Q. J. Seismol.* 81 (2017), 1–7. https://www.jma.go.jp/jma/kishou/books/kenshin/vol81_9.pdf.
- Heidarzadeh, M., Satake, K., 2013. Waveform and spectral analyses of the 2011 Japan tsunami records on tide gauge and DART stations across the Pacific Ocean. *Pure Appl. Geophys.* 170, 1275–1293. <https://doi.org/10.1007/s00024-012-0558-5>.
- Heidarzadeh, M., Satake, K., 2014. Excitation of basin-wide modes of the Pacific Ocean following the March 2011 Tohoku tsunami. *Pure Appl. Geophys.* 171, 3405–3419. <https://doi.org/10.1007/s00024-013-0731-5>.
- Heidarzadeh, M., Murotani, S., Satake, K., Ishibe, T., Gusman, A.R., 2016. Source model of the 16 September 2015 Illapel, Chile, Mw 8.4 earthquake based on teleseismic and tsunami data. *Geophys. Res. Lett.* 43, 643–650. <https://doi.org/10.1002/2015GL067297>.
- Ho, T.-C., Satake, K., Watada, S., 2017. Improved phase corrections for transoceanic tsunami data in spatial and temporal source estimation: Application to the 2011 Tohoku earthquake. *J. Geophys. Res.* 122, 10,155–10,175. <https://doi.org/10.1002/2017JB015070>.
- Ho, T.-C., Satake, K., Watada, S., Fujii, Y., 2019. Source Estimate for the 1960 Chile Earthquake from Joint Inversion of Geodetic and Transoceanic Tsunami Data. *J. Geophys. Res.* 124, 2812–2828. <https://doi.org/10.1029/2018JB016996>.
- Honda, K., Terada, T., Yoshida, Y., Ishitani, D., 1908. Secondary undulations of oceanic tides. *J. Col. Sci. Imp. Univ. Tokyo* 24, 1–113. https://repository.dl.itc.u-tokyo.ac.jp/?action=pages_view_main&active_action=repository_view_main_item_detail&item_id=37838&item_no=1&page_id=28&block_id=31.
- Jankaew, K., Atwater, B.F., Sawai, Y., Choowong, M., Charoentitrat, T., Martin, M.E., Prendergast, A., 2008. Medieval forewarning of the 2004 Indian Ocean tsunami in Thailand. *Nature* 455, 228–231. <https://doi.org/10.1038/nature07373>.
- Japan Meteorological Agency, 1961. The report on the tsunami of the Chilean earthquake, 1960. In: Technical Report of JMA. 8. pp. 389. <http://tsunami-dl.jp/document/067>.
- Johnson, J.M., Satake, K., 1997. Estimation of seismic moment and slip distribution of the April 1, 1946, Aleutian tsunami earthquake. *J. Geophys. Res.* 102, 11765–11774. <https://doi.org/10.1029/97JB00274>.
- Johnson, J.M., Tanioka, Y., Ruff, L.J., Satake, K., Kanamori, H., Sykes, L., 1994. The 1957 great Aleutian earthquake. *Pure Appl. Geophys.* 142, 3–28. <https://doi.org/10.1007/BF00875966>.
- Johnson, J.M., Satake, K., Holdahl, S.R., Sauber, J., 1996. The 1964 Prince William Sound earthquake: Joint inversion of tsunami and geodetic data. *J. Geophys. Res.* 101, 523–532. <https://doi.org/10.1029/95JB02806>.
- Kagan, Y., Jackson, D.D., 2013. Tohoku earthquake: a surprise? *Bull. Seismol. Soc. Am.* 103 (2013), 1181–1194. <https://doi.org/10.1785/0120120110>.
- Kanamori, H., 1972. Mechanism of tsunami earthquakes. *Phys. Earth Planet. Inter.* 6, 346–359. [https://doi.org/10.1016/0031-9201\(72\)90058-1](https://doi.org/10.1016/0031-9201(72)90058-1).
- Kelleher, J.A., 1972. Rupture zones of large South American earthquakes and some predictions. *J. Geophys. Res.* 77, 2087–2103. <https://doi.org/10.1029/JB077i01p02087>.
- Konno, E., Iwai, J., Takayanagi, Y., Nakagawa, H., Onuki, Y., Shibata, T., Mii, H., Kitamura, N., Kotaka, T., Kataoka, J., 1961. Geological survey report along Sanriku coast damaged by Chilean earthquake tsunami (in Japanese). *Contrib. Inst. Geol. Paleontol. Tohoku Univ.* 52, 1–45. <http://hdl.handle.net/10097/33142>.
- Kunitomi, S., 1933. On Sanriku strong earthquake and tsunami (in Japanese). *Q. J. Seismol.* 81 (2017), 111–153. <https://www.jma.go.jp/jma/kishou/books/kenshin/vol7p111.pdf>.
- La Selle, S., Richmond, B.M., Jaffe, B.E., Nelson, A.R., Griswold, F.R., Arcos, M.E.M., Chagué, C., Bishop, J.M., Bellanova, P., Kane, H.H., Lunghino, B.D., Gelfenbaum, G., 2019. Sedimentary evidence of prehistoric distant-source tsunamis in the Hawaiian Islands. *Sedimentology*. <https://doi.org/10.1111/sed.12623>.
- Macdonald, G.A., Shepard, F.P., Cox, D.C., 1947. The tsunami of April 1, 1946, in the Hawaiian Islands. *Pac. Sci.* 1, 21–37. <http://hdl.handle.net/10125/12536>.
- McCaffrey, R., 2008. Global frequency of magnitude 9 earthquakes. *Geology* 36, 263–266. <https://doi.org/10.1130/G24402A.1>.
- Milne, J., 1880. The Peruvian earthquake of May 9th, 1877. *Trans. Seism. Soc. Japan* 2, 50–96. <https://repository.dl.itc.u-tokyo.ac.jp/>.
- Morton, R.A., Goff, J.R., Nichol, S.L., 2008. Hydrodynamic implications of textural trends in sand deposits of the 2004 tsunami in Sri Lanka. *Sediment. Geol.* 207, 56–64. <https://doi.org/10.1016/j.sedgeo.2008.03.008>.
- Narayana, A.C., Tataravti, R., Shinu, N., Subeer, A., 2007. Tsunami of December 26, 2004 on the southwest coast of India: Post-tsunami geomorphic and sediment characteristics. *Mar. Geol.* 242, 155–168. <https://doi.org/10.1016/j.margeo.2007.03.012>.
- Ninomiya, S., 1960. Tsunami in Tohoku coast induced by earthquake in Chile - a chronological review - (in Japanese). *Tohokukenkyu* 10, 19–23.
- Okada, Y., 1985. Surface deformation due to shear and tensile faults in a half-space. *Bull. Seismol. Soc. Am.* 75, 1135–1154. <https://pubs.geoscienceworld.org/ssa/bssa/article/75/4/1135/118782>.
- Okal, E.A., Synolakis, C., Fryer, G.J., Heinrich, P., Borrero, J.C., Ruscher, C., Arcas, D., Guille, G., Rousseau, D., 2002. A field survey of the 1946 Aleutian Tsunami in the Far Field. *Seismol. Res. Lett.* 73, 490–503. <https://doi.org/10.1785/gssr.73.4.490>.
- Okal, E.A., Borrero, J.C., Synolakis, C.E., 2006. Evaluation of tsunami risk from regional earthquakes at Pisco, Peru. *Bull. Seismol. Soc. Am.* 96, 1634–1648. <https://doi.org/10.1785/0120050158>.
- Pelinovsky, E., Choi, B.H., Stromkov, A., Didenkulova, I., Kim, H.-S., 2005. Analysis of tide-gauge records of the 1883 Krakatau tsunami. In: Satake, K. (Ed.), *Tsunami: Case Studies and Recent Developments*. Springer, pp. 57–78. <https://www.springer.com/gp/book/9781402033261>.
- Power, W., 2013. Review of tsunami hazard in New Zealand. update). GNS Science Consultancy Report 2013/131. <https://www.civildefence.govt.nz/cdem-sector/cdem-research-/mcdem-research-projects-and-resources/review-of-tsunami-hazard-in-new-zealand/>.
- Press, F., Harkrider, D., 1966. Air-sea waves from the explosion of Krakatoa. *Science* 154, 1325–1327. <https://doi.org/10.1126/science.154.3754.1325>.
- Rabinovich, A.B., Thomson, R.E., 2007. The 26 December 2004 Sumatra tsunami: Analysis of tide gauge data from the world ocean Part 1. Indian Ocean and South Africa. *Pure Appl. Geophys.* 164, 261–308. <https://doi.org/10.1007/s00024-006-0164-5>.
- Rabinovich, A.B., Thomson, R.E., Stephenson, F.E., 2006. The Sumatra tsunami of 26 December 2004 as observed in the North Pacific and North Atlantic oceans. *Surv. Geophys.* 27, 647–677. <https://doi.org/10.1007/s10712-006-9000-9>.
- Rabinovich, A.B., Titov, V.V., Moore, C.W., Eblé, M.C., 2017. The 2004 Sumatra tsunami in the Southeastern Pacific Ocean: New global insight from observations and modeling. *J. Geophys. Res. - Oceans* 122 (10), 7992–8019. <https://doi.org/10.1002/2017JC013078>.
- Rabinovich, A.B., Thomson, R.E., Krassovski, M.V., Stephenson, F.E., Sunnott, D.C., 2019. Five great tsunamis of the 20th century as recorded on the coast of British Columbia. *Pure Appl. Geophys.* 176, 2887–2924. <https://doi.org/10.1007/s00024-019-02133-3>.
- Rong, Y., Jackson, D.D., Magistrale, H., Goldfinger, C., 2014. Magnitude limits of subduction zone earthquakes. *Bull. Seismol. Soc. Am.* 104, 2359–2377. <https://doi.org/10.1785/0120130287>.
- Saito, T., Inazu, D., Tanaka, S., Miyoshi, T., 2013. Tsunami coda across the Pacific Ocean following the 2011 Tohoku-Oki Earthquake. *Bull. Seismol. Soc. Am.* 103, 1429–1443. <https://doi.org/10.1785/0120120183>.
- Satake, K., 1988. Effects of bathymetry on tsunami propagation - application of ray tracing to tsunamis. *Pure Appl. Geophys.* 126, 27–36. <https://doi.org/10.1007/BF00876912>.
- Satake, K., 2014. Advances in earthquake and tsunami sciences and disaster risk reduction since the 2004 Indian ocean tsunami. *Geosci. Lett.* 1, 15. <https://doi.org/10.1186/s40562-014-0015-7>.
- Satake, K., 2015a. Tsunamis. In: Schubert, G. (Ed.), *Treatise on Geophysics*, Second edition. Vol. 4. Elsevier, pp. 477–504. <https://doi.org/10.1016/B978-0-444-53802-4.00086-5>.
- Satake, K., 2015b. Geological and historical evidence of irregular recurrent earthquakes in Japan. *Phil. Trans. R. Soc. A* 373, 2014375. <https://doi.org/10.1098/rsta.2014.0375>.
- Satake, K., Atwater, B.F., 2007. Long-term perspectives on giant earthquakes and tsunamis at subduction zones. *Annu. Rev. Earth Planet. Sci.* 35, 349–374. <https://doi.org/10.1146/annurev.earth.35.031306.140302>.
- Satake, K., Shimazaki, K., Tsuji, Y., Ueda, K., 1996. Time and size of a giant earthquake in Cascadia inferred from Japanese tsunami records of January 1700. *Nature* 379, 246–249. <https://doi.org/10.1038/379246a0>.
- Satake, K., Wang, K., Atwater, B.F., 2003. Fault slip and seismic moment of the 1700 Cascadia earthquake inferred from Japanese tsunami descriptions. *J. Geophys. Res.* 108, B11 2535. <https://doi.org/10.1029/2003JB002521>.
- Schurr, B., Asch, G., Hainzl, S., Bedford, J., Hoehn, F., Palo, M., Wang, R., Moreno, M., Bartsch, M., Zhang, Y., Oncken, O., Tilmann, F., Dahm, T., Victor, P., Barrientos, S., Vilotte, J.-P., 2014. Gradual unlocking of plate boundary controlled initiation of the 2014 Iquique earthquake. *Nature* 512, 299–302. <https://doi.org/10.1038/nature13681>.
- Shuto, N., 1991. Numerical simulation of tsunamis - its present and near future. *Nat. Hazards* 4, 171–191. <https://doi.org/10.1007/BF00162786>.
- Simkin, T., Fiske, R., 1983. *Krakatau, 1883 - The Volcanic Eruption and its effects*. Smithsonian Institution Press, pp. 464.
- Smith, W.H.F., Scharroo, R., Titov, V.V., Arcas, D., Arbic, B.K., 2005. Satellite altimeters measure tsunami, early model estimates confirmed. *Oceanography* 18, 11–13. <https://doi.org/10.5670/oceanog.2005.62>.
- Titov, V., Rabinovich, A.B., Mofjeld, H.O., Thomson, R.E., González, F.I., 2005. Global Reach of the 26 December 2004 Sumatra Tsunami. *Science* 309, 2045–2048. <https://doi.org/10.1126/science.1114576>.
- Tsuji, Y., 2013. Catalog of distant tsunamis reaching Japan from Chile and Peru. *Res. Rep. Tsunami Eng.* 30, 61–68. http://www.tsunami.civil.tohoku.ac.jp/hokusai3/J/publications/pdf2/vol30_8.pdf.
- Tsuji, Y., Satake, K., Ishibe, T., Harada, T., Nishiyama, A., Kusumoto, S., 2014. Tsunami heights along the Pacific Coast of northern Honshu recorded from the 2011 Tohoku and previous great earthquakes. *Pure Appl. Geophys.* 171, 3183–3215. <https://doi.org/10.1007/s00024-014-0779-x>.
- Villegas-Lanza, J.C., Chlieh, M., Cavalie, O., Tavera, H., Baby, P., Chire-Chira, J., Nocquet, J.M., 2016. Active tectonics of Peru: Heterogeneous interseismic coupling

- along the Nazca megathrust, rigid motion of the Peruvian Sliver, and Subandean shortening accommodation. *J. Geophys. Res.* 121, 7371–7394. <https://doi.org/10.1002/2016JB013080>.
- Watada, S., Kusumoto, S., Satake, K., 2014. Traveltime delay and initial phase reversal of distant tsunamis coupled with the self-gravitating elastic Earth. *J. Geophys. Res.* 119, 4287–4310. <https://doi.org/10.1002/2013JB010841>.
- Watanabe, H., 1972. Statistical studies on the wave-form and maximum height of large tsunamis. *J. Ocean. Soc. Japan* 28, 229–241. <https://doi.org/10.1007/BF02109293>.
- Yamazaki, Y., Cheung, K.F., 2011. Shelf resonance and impact of near-field tsunami generated by the 2010 Chile earthquake. *Geophys. Res. Lett.* 38, L12605. <https://doi.org/10.1029/2011GL047508>.
- Yoshimoto, M., Kumagai, H., Acero, W., Ponce, G., Váscónez, F., Arrais, S., Ruiz, M., Alvarado, A., García, P.P., Dionicio, V., Chamorro, O., Maeda, Y., Nakano, M., 2017. Depth-dependent rupture mode along the Ecuador-Colombia subduction zone. *Geophys. Res. Lett.* 44, 2203–2210. <https://doi.org/10.1002/2016GL071929>.
- Yuan, X.H., Kind, R., Pedersen, H.A., 2005. Seismic monitoring of the Indian ocean tsunami. *Geophys. Res. Lett.* 32, L15308. <https://doi.org/10.1029/2005GL023464>.